An MD simulation of the decoy action of Epstein–Barr virus LMP1 protein mimicking the CD40 interaction with TRAF3

Chung, Wilfredo Credo; Ishida, Toshimasa

An MD simulation of the decoy action of Epstein-Barr virus LMP1 protein mimicking the CD40 interaction with TRAF3

Wilfredo Credo Chung • Toshimasa Ishida

Fukui Institute for Fundamental Chemistry, Kyoto University,
34-4, Takano-nishihirakicho, Sakyo-ku, Kyoto 606-8103, Japan
Corresponding author: T. Ishida (ishida@fukui.kyoto-u.ac.jp)

Abstract The Epstein-Barr virus (EBV) is associated with a variety of malignancies and chronic active EBV infection is a severe systemic disease associated with high rates of mortality and morbidity. In this paper, the dynamics of the interaction of EBV-expressed latent membrane protein 1 (LMP1) with cellular signaling intermediate tumor necrosis factor receptor (TNFR)-associated factor 3 (TRAF3) is simulated using standard classical molecular dynamics (MD) protocols. For comparison, the dynamics of the interaction of TRAF3 with CD40, a TNFR mimicked by LMP1 to effect EBV infection is also calculated under similar conditions. Essential dynamics (ED) analysis is carried out to identify important degrees of vibrational freedom that relate to protein function and virus infection. Both the MD simulation and ED analysis reveal novel interactions that help explain the structural decoy action of LMP1 over CD40. These interactions involve the consensus sequence PXQXTXX shared by CD40 and LMP1. In LMP1, we have found novel interaction of Asp 209 with TRAF3 and the interaction is crucial although the adjacent Asp 210 was suggested to be essential by the X-ray analysis. In CD40, it is found that the hairpin formation is not indispensable for the interaction with TRAF3.

Keywords *Epstein-Barr virus • Essential dynamics • Molecular dynamics • TRAF3 • LMP1 • CD40*

1 Introduction

The Epstein-Barr virus (EBV) is a herpes virus that is the major cause of infectious mononucleosis [1]. It is known to infect the salivary gland cells and the B lymphocyte. In the salivary gland cells the virus growth cycle is completed whereas in the B lymphocyte the virus cycle is abortive. Even in the latter case, the affected B lymphocytes can multiply excessively to produce a cancer to the lymphatic system. The EBV is associated with a variety of malignancies including African lymphoid cancer, nasopharyngeal carcinoma, encephalitis, paralyses of various nerve groups and hydroa vacciniforme (HV) [2], a photosensitivity disorder in children characterized by vesiculopapules on sun-exposed areas that usually disappears by early adult life [3,4]. The HV lesions are usually induced by sunlight and UV radiation. There are no specific treatments of any form of EBV infection and no vaccine has yet been developed. Chronic active EBV infection is a severe systemic disease associated with high rates of mortality and morbidity [5].

EBV-encoded latent membrane protein 1 (LMP1) is the major transforming protein of EBV. LMP1 transforms primary B lymphocytes into lymphoblastoid cell lines [6]. To help EBV evade the cell death machinery of the human host, LMP1 mimics the tumor necrosis factor receptor (TNFR) CD40 [7].

CD40 is a costimulatory protein that, after ligation, interacts with a cellular signaling intermediate, tumor necrosis factor receptor-associated factor III (TRAF3) to control B cell proliferation, growth and differentiation [8-10]. TRAF3 is one of six tumor necrosis factor receptor-associated factor proteins that connect TNFRs to downstream signaling pathways [11-14].

LMP1 is also known to bind to the intracellular TRAF3 for the decoy action. Only a few selected sites of the cytoplasmic domain carboxyl terminus (CCT) of LMP1 are essential for B lymphocyte transformation [15]. The LMP1 binds to TRAF3 using its CCT site.

X-ray analysis of the LMP1-TRAF3 and CD40-TRAF3 were reported by Wu et al. [16] and Ni et al. [17], respectively. CD40, CD30 and LMP1 bind with TRAFs 1-3 through a common sequence PXQX(T/S). In CD40, the sequence is ^{250}PVQET^{254} [17] and in LMP1, the sequence is ^{204}PQQAT^{208}. Both the sequences bond to the same hydrophobic binding crevice of TRAF3. The Based on the X-ray analysis, CD40 binds to TRAF3 and initiate several transduction pathways [17]. CD40-TRAF3 specific contacts has been investigated [17-19]. Ni et al. found the hairpin formation in CD40-TRAF3 complex and suggested that the formation is indispensable for the interaction with TRAF3. Wu et al. claimed that Asp 210 was the key residue in LMP1 because Asp 210 had unique contacts with TRAF3 and because the corresponding contacts were not found in CD40-TRAF3.

It is not trivial, however, that the interactions found in X-ray crystallography is the real ones under biological conditions although an X-ray result provides us one unique ‘clear-cut’ picture. Some important interactions in fluctuating biological systems can be overlooked. Thus, the MD simulation would be complementary tool to investigate the movement in real systems. In this paper, we will carry out molecular dynamics simulations to investigate whether the interactions

suggested in X-ray studies are still relevant under biological conditions and whether novel interactions are responsible for the decoy action of LMP1 in EBV. We also perform the essential dynamics to identify important structural distortions in CD40 and LMP1 that relate to binding with TRAF3 and structural decoy action.

The method of essential dynamics (ED) [20] separates a few essential collective degrees for freedom that are relevant to the function of the protein from irrelevant local fluctuations. It is an eigensystem analysis of covariant matrix of positional deviations wherein two configurational subspaces are constructed by a linear transformation of the covariance matrix of positional deviations. By doing so, ED can identify large concerted structural rearrangements from unimportant fluctuations in a multiparticle system.

The succeeding sections are organized as follows: first, a detailed methodology will be outlined; then, we will present MD results, discuss CD40-TRAF3 interactions, LMP1-TRAF3 interactions, compare root mean square deviation of the two complexes from their respective optimized structure, and carry out essential dynamics analysis based on the MD trajectories. Based on the results, we describe an implication for the vaccine development. The article will be closed by an enumeration of conclusions.

2 Methodology

In an effort to better understand the mechanism of the decoy action of LMP1, the system was subjected to classical MD trajectory simulation. Initial complexes of TRAF3 with LMP1 and CD40 were derived from Protein Data Bank crystal structures 1ZMS [16] and 1FLL [17], respectively. 1ZMS has monomer structure with one TRAF3 and one LMP1 subunit whereas 1FLL is a dimeric structure of two TRAF3 (chains A and B) and CD40 (chains X and Y) subunits identical to each other. Thus, we used only chains A and X of 1FLL for our simulation. Hydrogen atoms are added automatically using the LEaP utility of the Amber 9 suite of MD programs and utilities [21,22].

The residue numbering employed is presented in Table 1. Within the PDB structure 1ZMS, the structurally-resolved sequence of LMP1 consists only of 7 residues (204-210, sequence PQQATDD) whereas that of CD40 in 1FLL is 21 (residue 246-266). To make the two even, we extended the LMP1 structure by manually adding the missing residues. This treatment would prevent the “terminal” residues of LMP1 to have artificial flexibility. When the LMP1 chain was extended, we assumed that LMP1 also imitated the hairpin configuration of CD40 and so the missing residues were built in this way. Four residues (200-203, sequence LPHP) were added to the N terminus of LMP1 while 10 residues (211-220, sequence SGHESDSNEG) were attached to the C terminus to make it as long as that of CD40 in 1FLL. The consensus sequence PXQXT is numbered 250-254 in CD40 whereas they are residues 204- 208 in LMP1. There are 13 residues missing in the TRAF3 sequence in 1ZMS (residue number 313-504) when compared to TRAF3 in 1FLL (residue number 300-504). We did not try to simulate the missing residues since they are located far from the interaction region in TRAF3.

The complexes were solvated with the TIP3P [23] water molecules and neutralized with chloride ions. Periodic boundary conditions were applied where the box encloses the entire atoms. A 10-Å buffer zone on each direction was imposed. Initially, the entire protein was kept frozen and only the energy of the water molecules was minimized. Subsequently, the energy of the whole system was minimized. The system was then slowly heated to 300 K over a period of 10 ps in the canonical (NVT) ensemble. The system density was then equilibrated at constant pressure and temperature (NPT) to a final density around 1 g/cm^3. It took 200 ps for the density to stabilize. Production MD runs were done at 300 K for 66 ns in the NPT ensemble. The trajectory points were recorded every 1 ps and the trajectory within the last 16 ns were analyzed for ED. The structure after energy minimization of the whole system was used as the reference structure for the ED analysis.

In addition to the long-time (66 ns) trajectory, six short-time (2 ns) trajectories were also calculated to check if the long-time trajectory is not extraordinary. The short-time trajectories were analyzed in the same way as the 66-ns trajectory except for the ED analysis which was no longer done on the 2-ns trajectories. The results from the abbreviated trajectory runs are presented in the Supplementary Information section.

The basic force field parameters were derived from Wang et al.'s Amber 1999 force fields [24] while the amino acid parameters were derived from Cornell et al.'s Amber 1994 amino acid database [25]. Collectively, the parameter set utilized in this simulation is routinely referred to as the ff99 force field. All histidine residues are built in their protonated form. The simulations were done using Amber 9 [21,22].

3 Results and Discussion

3.1 CD40-TRAF3 interactions

Fig. 1 shows structures of CD40, where panel (a) is the averaged structure in the MD simulation and panel (b) is the X-ray structure in the previous work [17]. Fig. 2 is the temporal profile of some important intra- and intermolecular hydrogen bonds* made by CD40 with TRAF3. We have found that under the conditions employed in this MD simulation, the contacts made by CD40 with

* Hydrogen bonds are identified with the aid of the FindHBond utility in Chimera [26] which uses atom types and geometric criteria. Hydrogen bonds are identified even when hydrogen atoms are not present. The geometric criteria are described in reference [27]. Possible donor groups are hydrogen-bearing nitrogen, oxygen, and sulfur atoms, and possible acceptor groups are nitrogen, oxygen, and sulfur atoms with a lone pair. H-bonds involving other types of atoms are not considered. For X-ray structures, hydrogen bonds were identified prior to the addition of hydrogen atoms. In the case of MD simulated structures, hydrogen atoms were present when hydrogen bond interactions were scanned. However, the interatomic distances monitored are those between the acceptor atom and the hydrogen-bearing donor heavy atom.

TRAF3 are quite different compared to that deduced from the X-ray crystal structure as described below.

The intramolecular hydrogen bond between Thr 254 and Glu 264 is severed (Fig. 1a; see also green line, Fig. 2a) whereas, in the X-ray structure, this hydrogen bond is one of the two intracellular hydrogen bonds that stabilize the hairpin configuration, the other one being that between Thr 254 and Asp 265 (Fig. 1b). Consequently, all of the contacts made by Gln 263 with TRAF3 (at Tyr 395 and Asp 399) are also severed, which causes Gln 263's orientation to be flexible (red and blue lines, Fig. 2a). Ni et al. claimed that these contacts were critical for CD40/TRAF3 recognition and that the CD40 fragment assumed a hairpin configuration when the fragment is bound to TRAF3. The present MD simulation, however, shows the contacts are easy to break. The simulation result also indicates that the hairpin structure is not necessarily essential because three hydrogen bonds between CD40 and TRAF3 are still revealed without the hairpin structure, as seen in Fig. 1(a) and Table 2(a).

Val 251 and Glu 253 are within the consensus sequence PXQXT shared by CD40 and LMP1 and are positioned at residues X, which means these two amino residues are mutated from CD40 to LMP1. Thus, these two residues are very important to examine the decoy action by LMP1. Val 251's hydrogen bond with Ser 468, which exists in the X-ray structure but not mentioned explicitly by Wu et al, is destroyed (red line, Fig. 2b) and the former makes an apparently stronger bidentate-type hydrogen bond interaction with Gly 469 (green and blue lines, Fig. 2b). Also, Glu 253 comes within hydrogen bond distance with Ala 467 in TRAF3 (purple line, Fig. 2b). These two interactions are backbone-backbone interactions. Side chain atoms do not play a direct role in these interactions.

Thus, the present MD simulation under thermally-equilibrated and solvated conditions indicates that Val 251 and Glu 253 are important residues that bring about recognition of CD40 by TRAF3 and initiation of the signaling cascade. This is quite different from the mechanism deduced from the X-ray structure where CD40's Gln 263 plays a central role in molecular recognition with TRAF3 and the hairpin configuration is essential. The hydrogen bonds revealed by the MD simulation make more intuitive sense than the ones deduced from the X-ray structure because the contacts include the mutated amino residues in the consensus sequence.

In the X-ray-structure, CD40's Lys 246, Thr 247 and Val 251 comes within hydrogen bond distance with TRAF3's Lys 449, Asp 451 and Ser 468, respectively, (Fig. 1b) although Wu et. al did not refer to their importance. These hydrogen bonds are not found in the present MD simulation. In the X-ray analysis shows Pro 250 also makes an intramolecular hydrogen bond with Gln 252, but this intramolecular interaction is not found in the MD simulation, either.

3.2 LMP1-TRAF3 interactions

Fig. 3 shows structures of LMP1, where panel (a) is the averaged structure in the MD simulation panel (b) is the X-ray structure in the previous work [16]. Fig. 4 shows the temporal profile of some important intra- and intermolecular hydrogen bonds made by LMP1 with TRAF3. Under

solvated and thermally-equilibrated conditions, LMP1 Gln 206's hydrogen bonds with TRAF3 Ser 454 and Ser 456 are destroyed (red line, Fig. 4a; blue line Fig. 4b) whereas, in their X-ray experiment, Wu et al. [16], reported that LMP1's Gln 206 makes a hydrogen bond with Ser 454 and is within hydrogen-bonding distance with Ser 456 (Fig. 3b). Gln 206 is the same amino acid residue as Gln 252 in CD40 in the motif sequences and thus is not expected to be important to virus decoy action. Gln 206 does not make any hydrogen bond with other TRAF3 residues after its contacts are broken. On the other hand, Thr 208's hydrogen bonds with Asp 399 are preserved (green and purple lines, Fig. 4b).

The hydrogen bonds made by Asp 210 are also destroyed during the MD simulation (blue and purple lines, Fig. 4a). Wu et. al., from their X-ray crystallographic studies, suggested that LMP1's Asp 210 form a hydrogen bond with TRAF3's Tyr 395 and Arg 393 (Fig. 3b). They claimed that, in effect, LMP1's Asp 210 was a key residue in the structural decoy action and that an equivalent contact in the CD40-TRAF3 complex was not found [16]. However, the hydrogen bond is destroyed in the present MD simulation. Thus, the importance of the alleged unique contact made by Asp 210 that does not have an equivalent in CD40 should be reexamined.

Instead of the two severed interactions, Asp 209 in LMP1 comes within hydrogen bond distances with Arg 393 in TRAF3, which was hydrogen-bonded to Asp 210 in the X-ray crystallography structure (Fig. 3a; see also red line, Fig. 4c). This novel hydrogen bond interaction made by Asp 209 is more realistic than that by Asp 210 since Asp 210 involves the ‘artificial’ terminal oxygen atom in the X-ray structure. Asp 210 is not actually one of the terminal residues and is just a terminal one resolved in the X-ray analysis. In the MD simulation, unresolved parts of LMP1 chain is extended as described in Methodology Section and the artificial terminal oxygen is replaced with the peptide bond to the next amino acid. Asp 209's side-chain carboxyl oxygen OD1 is, on the average, about 2.59 Å away from one of Arg 393's guanidino hydrogen although this hydrogen bond is at times broken, in particular during the early phase of the dynamics.

Two residues, Gln 205 and Ala 207, in LMP1, which correspond to Val 251 and Glu 253 in CD40, are different in the consensus 5-residue sequence, P(V/Q)Q(E/A)T. The two residues are, therefore, presumably crucial to the decoy action and have their hydrogen bond interaction with TRAF3. Gln 205 has a bidental hydrogen bond network with Gly 469 (Fig. 3a; see also blue and green lines, Fig. 4c) and Ala 207 has a hydrogen bond with Ala 467(Fig. 3a; see also purple line, Fig. 4c). These two interactions are also found in the X-ray structure although the latter was not reported by Wu et al. We note that the interaction of these two residues involve backbone atoms rather than side chain atoms, which is similar to the situation observed in the CD40-TRAF3 MD-averaged complex except that the residue combinations are different (Gln-Gly and Ala-Ala for LMP1-TRAF3 whereas it is Val-Gly and Glu-Ala in CD40-TRAF3).

It is noted that neither the hydrogen bonds made by Gln 206 nor Thr 208 are seen in the MD simulation in addition that the ones by Asp 210 are not whereas these bonds were recognized in the X-ray crystallographic structure, as shown in Table 2(b).

3.3 Comparison of root mean square (RMS) deviation of the two complexes from their respective optimized structure.

In this subsection, the RMS deviation (RMSD) of the CD40-related structures and LMP1-related ones from the corresponding minimized structures are compared to gage the extent of interaction with TRAF3. We compared the RMSD (a) of LMP1-TRAF3 with CD40-TRAF3, (b) of LMP1 with CD40, and (c) of the seven corresponding important residues in LMP1 with those in CD40. The movement of the atoms not belonging to the chosen subset is ignored. The reference structure is always the energy-minimized solvated and neutralized complex.

The plot shown in Fig. 5a clearly demonstrates the greater affinity of LMP1-TRAF3 (red curve) with an RMSD of around 12 Å at most compared to that of the CD40-TRAF3 complex that is about twice greater (green curve). However, this analysis is of limited value due to its very broad scope. For instance it includes the movement of the tail part of TRAF3 which can be very flexible yet its flexibility has little or no consequence to the function of TRAF3.

In Fig. 5b, the RMSD of the whole CD40 and LMP1 chains with respect to the minimized structure are also compared. Most of the time, the plot shows greater interaction between the virus protein with TRAF3 except for the period between ~35 ns to ~55 ns wherein it would appear that CD40 is bound more strongly to TRAF3. However, the interpretation of this plot should be done with caution since the LMP1 X-ray structure was extended manually and that the results plotted in Fig. 5b carries this artifact. Nevertheless, comparing the average RMSD over the simulation period still indicates that LMP1 (average RMSD = 6.16 Å) interacts more strongly than CD40 (average RMSD = 7.52 Å) supporting the experimentally observed decoy action of LMP1.

Shown in Fig. 5c is a comparison of the RMSD of the PXQXTXX motif of both CD40 and LMP1 with the energy-minimized structure as reference. It is clearly shown in this graph that the PQQATDD motif in LMP1 is more strongly attached to TRAF3 compared to the PVQETLH motif in CD40. The average RMSD of PQQATDD is only 2.22 Å while that of PVQETLH is 2.72 Å, indicating lesser flexibility of the former due to stronger affinity with TRAF3. This is consistent with the observed decoy action of LMP1 over CD40 during virus infection.

We have established, from a macroscopic down to a microscopic point of view, that under aqueous conditions at 300 K, LMP1 can compete with CD40 for interaction with TRAF3 and initiate a complex sequence of signal transduction processes leading to symptoms of Epstein-Barr virus infection.

3.4 Essential Dynamics

In an effort to identify the most relevant motions that relate to signal transduction by CD40 and LMP1, an essential dynamics analysis was carried out as described in the Methodology section.

Shown in Fig. 6 is the RMS fluctuation of atoms for the eigenvector with the largest eigenvalue, that is, the most relevant nonlocal mode. Low points in this plot means greater affinity to the host TRAF3 presumably related to the function of the protein. It is unambiguously shown in this plot

that the principal component of the PQQATDD in LMP1 (red line) is more constrained than that of PVQETLH (green line). It is quite clear that LMP1's principal component offers less flexibility indicating that LMP1 is able to compete with CD40 during virus infection.

With the exception of several atoms in Gln 205, the RMS fluctuation of atoms within the PQQATDD sequence in LMP1 is almost always lower than that of PVQETLH atoms. Even the significantly large RMSF of most of the Gln 205 atoms does not necessarily mean that it has less affinity to TRAF3 than Val 251. A close inspection of the high points within Gln 205 reveals that these belong to the side chain atoms. We recall our previous observation that Gln 205 and its CD40 counterpart Val 251 form a hydrogen bond network with Gly 469 in TRAF3 though backbone atoms N and O. Thus, the side chain of these residues are actually flexible and that their flexibility is of little or no consequence to the interaction of the residue with Gly 469 in TRAF3.

Within the consensus sequence PXQXT, substitution of Glu 253 in CD40 by Ala 207 significantly improves binding with TRAF3 as showed by the lower RMSF of Ala 207 atoms (Fig. 6). Neighboring residues Gln 206 and Thr 208 also show increased affinity with TRAF3 even though they are conserved in the structural decoy action. We attribute this to some kind of an effect like that of a tether wherein the flexibility of neighboring residues or atoms are limited by the affinity of residues or atoms close to it. In this case, we argue that the limited flexibility of the tethered residues Gln 205 and Ala 207 limits the flexibility of conserved residues Pro 204, Gln 206 and Thr 208 as well.

Mutations of Leu 255 to Asp 209 and of His 256 to Asp 210, respectively, also enhance the affinity of LMP1 towards TRAF3 as shown by the low RMSF of these residues. In particular, mutation to Asp 210 play a more significant role. However, Asp 210 is not hydrogen-bonded to any TRAF3 residue, as shown in the MD average structure of Fig. 3a although the X-ray crystallographic study suggests that it does (Fig. 3b). On the other hand , Asp 209 forms a hydrogen bond with Arg 393 in TRAF3 albeit we have established earlier in subsection 3.2 that the bond is rather weak. Thus, we surmise that the ^{255}LH^{256} → ^{209}DD^{210} mutation is not critical to the structural decoy action of LMP1.

The essential dynamics of the structural decoy action of LMP1 over CD40 during Epstein-Barr virus infection is captured by the first eigenvector (that is, the one with the highest eigenvalue) as the other eigenvectors are relatively local modes. That is, the other eigenvectors represent motions that are inconsequential to the function of the biomolecule. Shown in Fig. 7 is the magnitude of the motion along the eigenvector obtained by projection of the trajectory onto first four eigenvectors. It can be seen that the first eigenvector represents a nonlocal mode with large displacements. On the other hand, starting with the second mode, the displacements become increasingly local. Thus, it is of little consequence to analyze the other modes aside from the first one.

3.5 Explanation on the natural selection of mutation sites in LMP1

We now formulate a rationale for LMP1's choice of mutation sites to be able to compete with CD40 by combining the molecular dynamics and essential dynamics results. Our analysis of the

MD results points to Val 251 → Gln 205 and Gln 253 → Ala 207 mutation as critical for the decoy action. The His 256 → Asp 210 and Leu 255 → Asp 209 substitutions appear inconsequential by virtue of Asp 209 and Asp 210's lack of stable interaction with TRAF3. Val 251 in CD40 and Gln 205 in LMP1 are hydrogen-bonded to the same residue (Gly 469) in TRAF3 through a bidentate-type hydrogen bond network of backbone residues. Gly 469 and Val 251 are both neutral nonpolar residues. Replacement of the nonpolar valine residue with a polar one as in the case of Gln 205 significantly distorts the electron density around the backbone atoms involved in hydrogen bonding. The result is a stronger hydrogen bond.

The substitution of Glu 253 in CD40 by Ala 207 significantly improves binding with TRAF3 as showed by the lower RMSF of Ala 207 atoms. This is due to the hydrogen-bond formation of Ala 207 in LMP1 with Ala 467 in TRAF3, which is shown in Fig. 3a and in Fig. 4c.The substitution would have produced a favorable configuration of Ala 207 with Ala 467 although Ala 207 in LMP1 is less polar than Glu 253 in CD40.

The above arguments provide the rationale for the residue mutation that occurs in LMP1 in a bid to compete with CD40 for interaction with TRAF3 in the EBV virus infection.

3.6 Implication to vaccine development

On basis of the present MD simulation upon the critical protein-protein interactions that initiate Epstein-Barr virus infection, a peptide vaccine that mimics LMP1 may be designed to provide immunity from the disease. In this, we should examine which residues in TRAF3 are important for interacting with CD40 or LMP1. From Table 2, it is found that Gly 469 and Ala 467 in TRAF3 play a pivotal role. Thus, it is suggested that the designer peptide should interact with TRAF3's Gly 469 and Ala 467 and stimulate antibody production from the patient but not cause severe infection at the same time. It is recommended that the synthetic peptide vaccine conserve P, Q and T in the PX_1QX_2T consensus sequence and the residues X_1 and X_2 be carefully chosen to bring about the desired immune response.

4 Conclusion

The complexes of TRAF3 with CD40 and LMP1 are subjected to standard MD simulation and essential dynamics analysis. MD simulation under solvated and thermally-equilibrated conditions reveal stable interactions that are not previously reported in X-ray diffraction studies. In LMP1, newly found interaction of Asp 209 with TRAF3 is relevant rather than Asp 210 found in the X-ray. In CD40, it is found that hairpin formation is not necessary for the interaction with TRAF3. Essential dynamics analysis reveal the most critical mutation in the decoy action. CD40's Val 251 and Glu 253 makes stable hydrogen bond interactions with TRAF3's Gly 469 and Ala 467, respectively. These interactions are not present in the X-ray structures 1FLL and 1ZMS. LMP1's polar residue Gln 205 replaces CD40's nonpolar residue Val 251 for a stronger interaction with TRAF3's Gly 469. The substitution of Glu 253 in CD40 by Ala 207 would have lead a favorable

configuration of Ala 207 with Ala 467 although Ala 207 in LMP1 is less polar than Glu 253 in CD40.

The interactions of TRAF3 with CD40 and LMP1 as well as the mechanism of the structural decoy action can be explained by studying hydrogen bond interactions. We also gave an implication to vaccine development on the basis of our results.

Acknowledgments The computations were performed using Research Center for Computational Science, Okazaki, Japan and Research Institute for Information Technology of Kyushu University. This research is partially supported by Grant-in-Aids for Scientific Research (C) No. 20608003 and (B) No. 19350013 from the Japan Society for the Promotion of Science (JSPS). WCC acknowledges the postdoctoral research fellowship at the Kyoto University Fukui Institute for Fundamental Chemistry and the Kyoto University Start-Up Grant for Young Scientists. Molecular graphics images were produced using the UCSF Chimera [26] package from the Resource for Biocomputing, Visualization, and Informatics at the University of California, San Francisco (supported by NIH P41 RR001081).

Tables

Table 1 Residue numbering of the protein complexes treated in this study

	1FLL (CD40-TRAF3)	1ZMS (LMP1-TRAF3)
TRAF3	300-504	313-504
CD40 or LMP1	246-266	200-220
PXQXT	250-254	204-208
PXQXTXX	250-256	204-210

Table 2 Relevant hydrogen bonds observed in the X-ray structure and MD simulation

(a) CD40-TRAF3

residues	Amber atom name of donor/acceptor heavy atoms involved[a]	
	MD simulation	X-ray structure
Val 251-Gly 469 (N-O)	√	None
Val 251-Gly 469 (O-N)	√	None
Val 251-Ser 468 (O-OG)	None	√
Glu 253-Ala 467 (N-O)	√	None
Glu 263-Asp399 (O-OD1)	None	√
Glu 263-Tyr 395 (OE1-OH)	None	√
Glu 264-Thr 254 (O-OG1)	None	√

(b) LMP1-TRAF3

residues	Amber atom name of donor/acceptor heavy atoms involved[a]	
	MD simulation	X-ray structure
Gln 205-Gly 469 (N-O)	√	√
Gln 205-Gly 469 (O-N)	√	√
Gln 206-Ser 456 (OE1-OG)	None	√
Gln 206-Ser 454 (OE1-OG)	None	√
Ala 207-Ala 467 (N-O)	√	√
Thr 208-Asp 399 (OG1-OD1)	√	√
Thr 208-Asp 399 (N-OD2)	√	√
Asp 209-Arg 393 (OD1-NH1)	√	None
Asp 210-Tyr 395 (OD2-OH)	None	√

[a] Standard Amber atom names are used: N = backbone amido N; O = backbone carbonyl O; OG = Ser hydroxyl O; OD1/OD2 = Asp side-chain carboxyl O; OE1 = Glu/Gln carboxyl O; OH = Tyr hydroxyl O; OG1 = Thr hydroxyl O

Figures

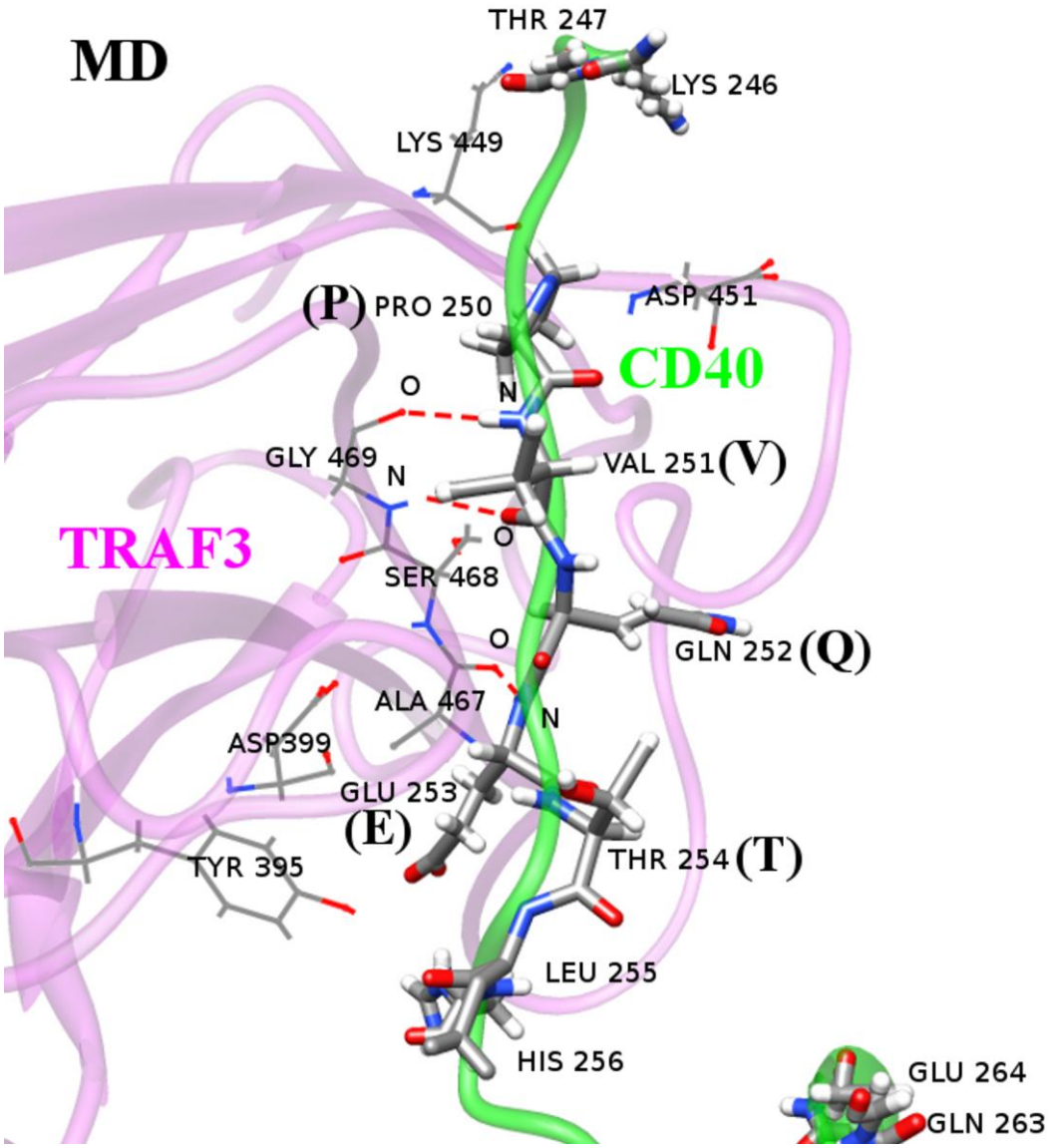

Fig. 1a

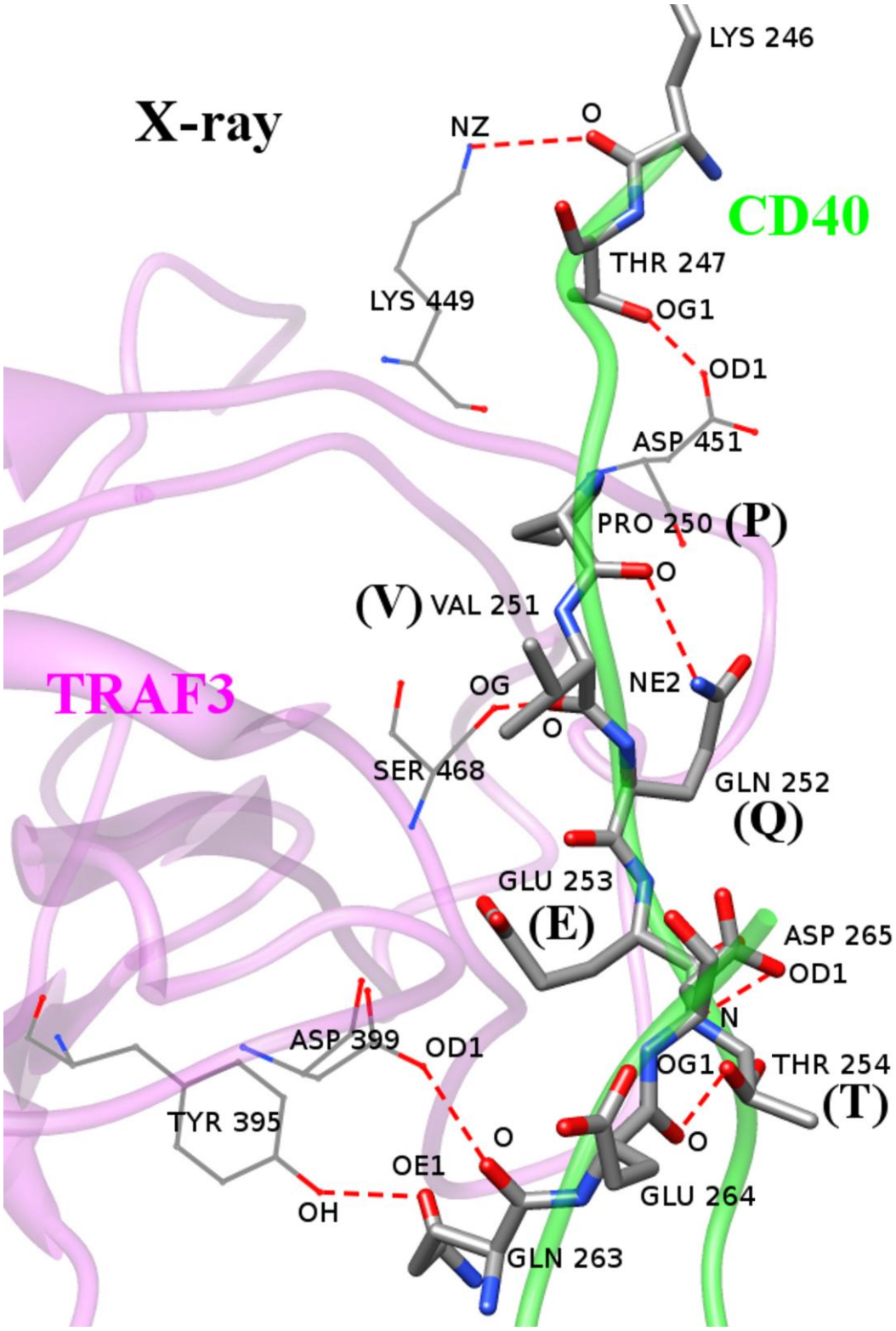

Fig. 1b

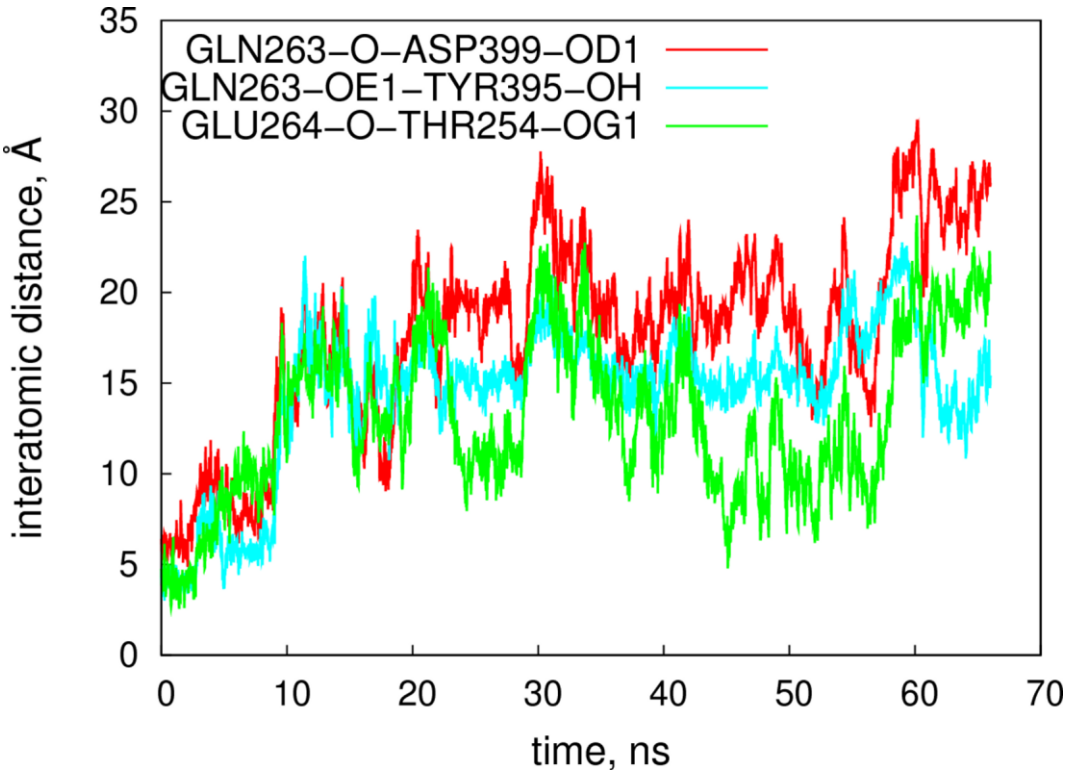

Fig. 2a

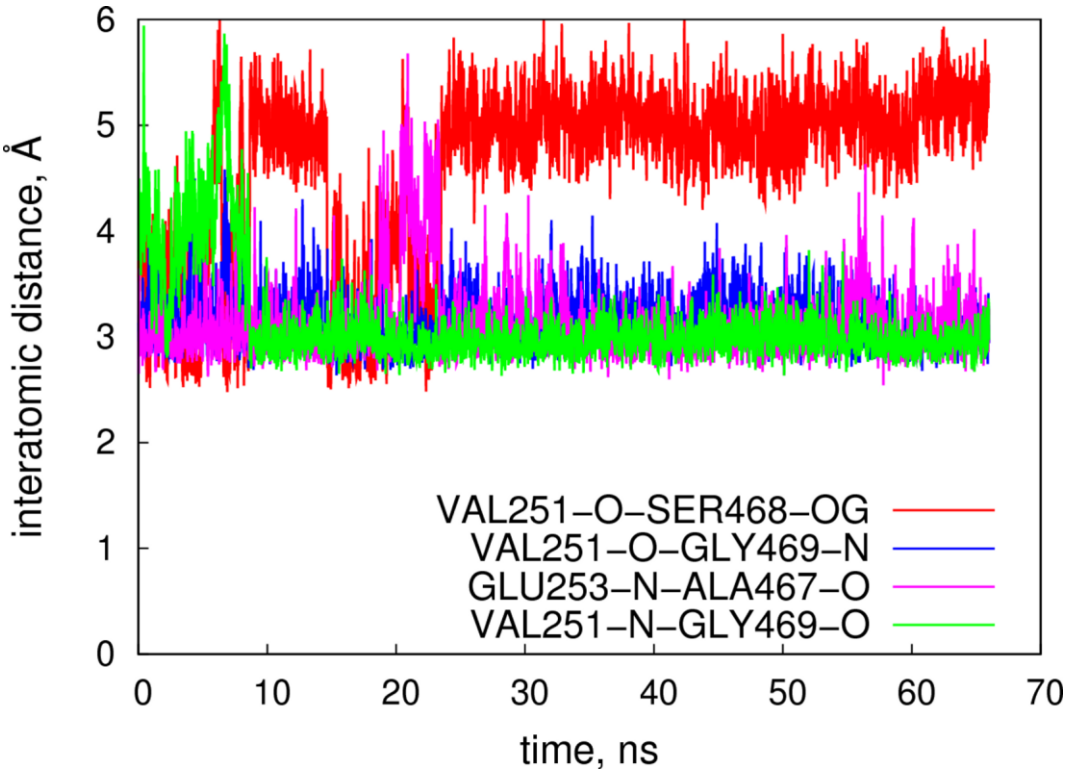

Fig. 2b

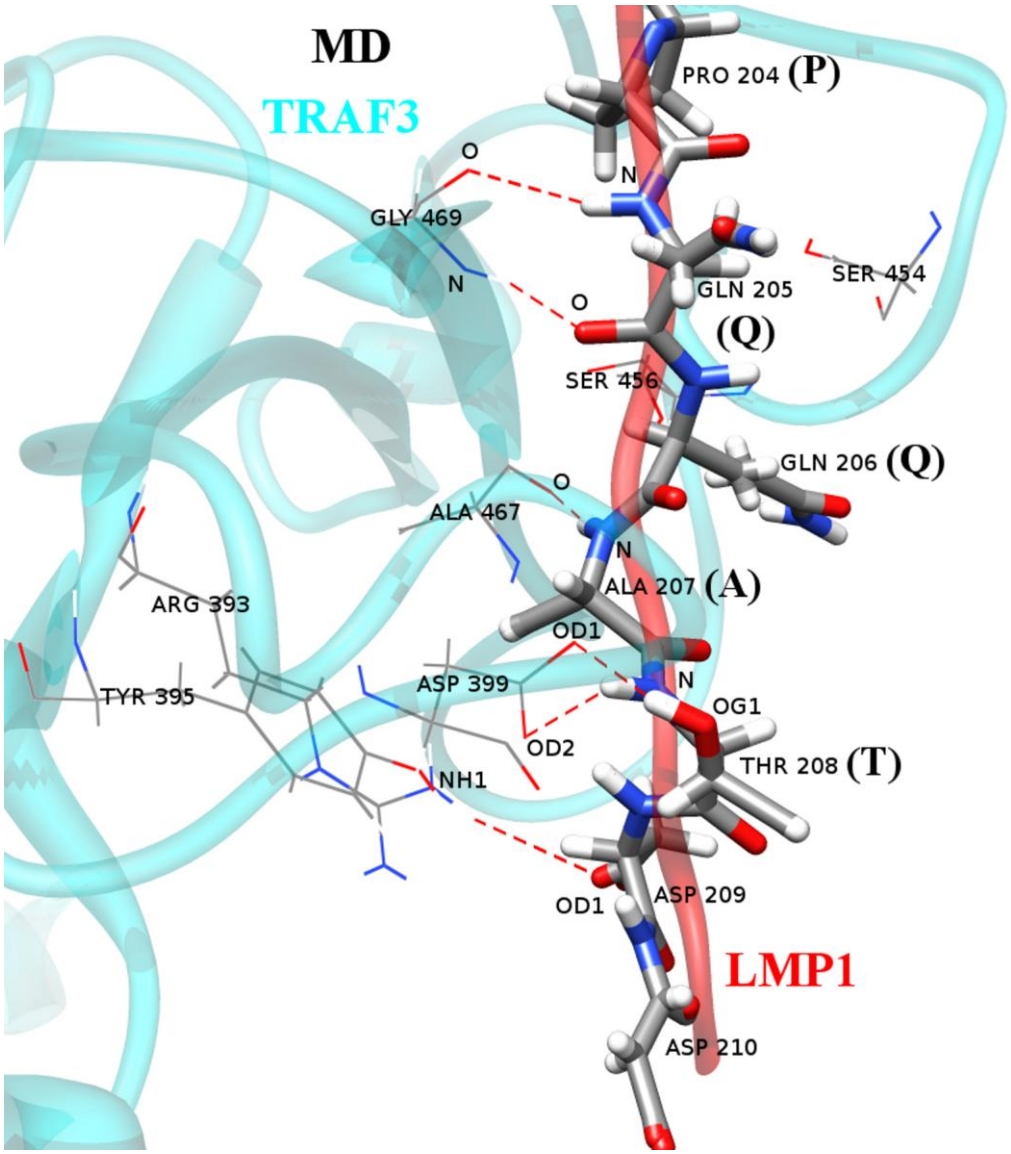

Fig. 3a

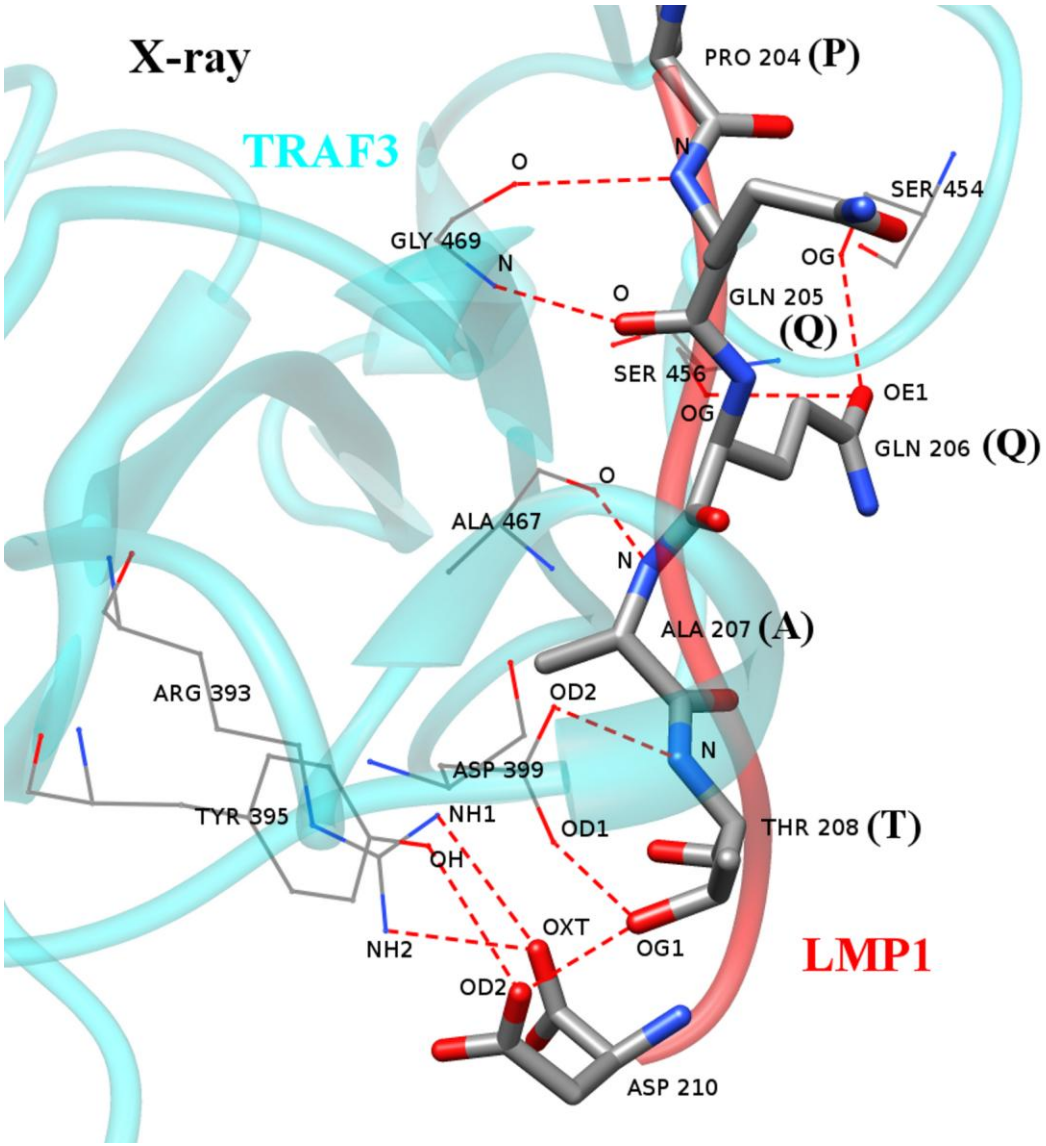

Fig. 3b

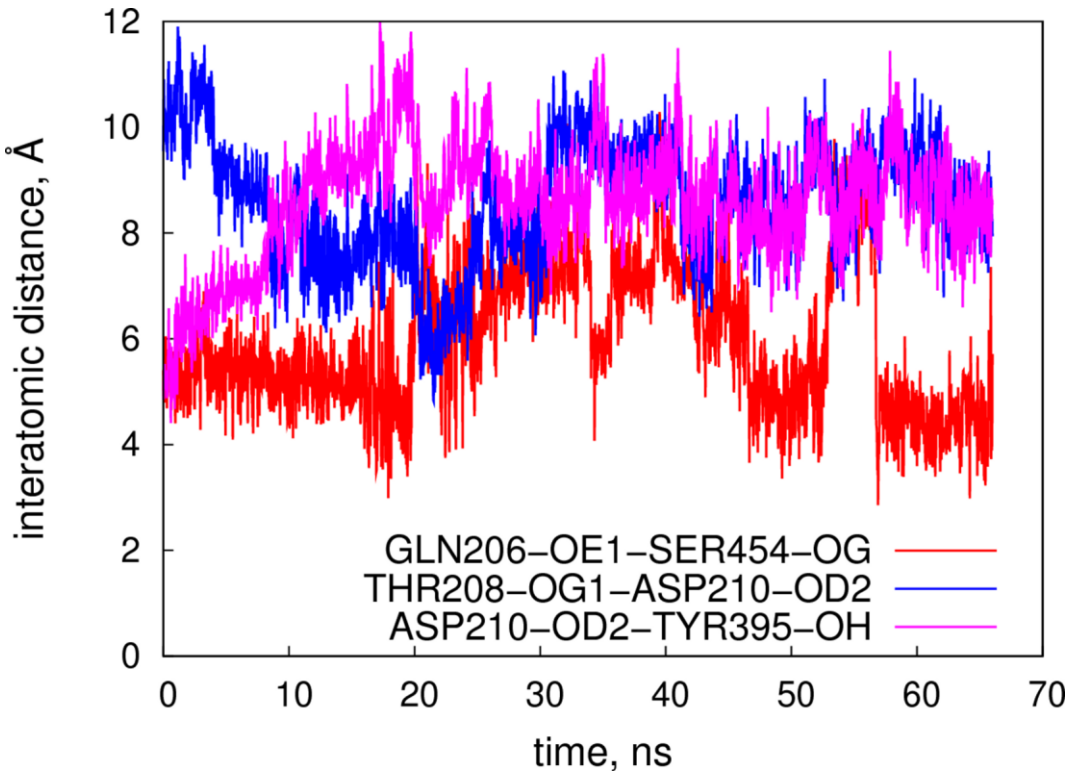

Fig. 4a

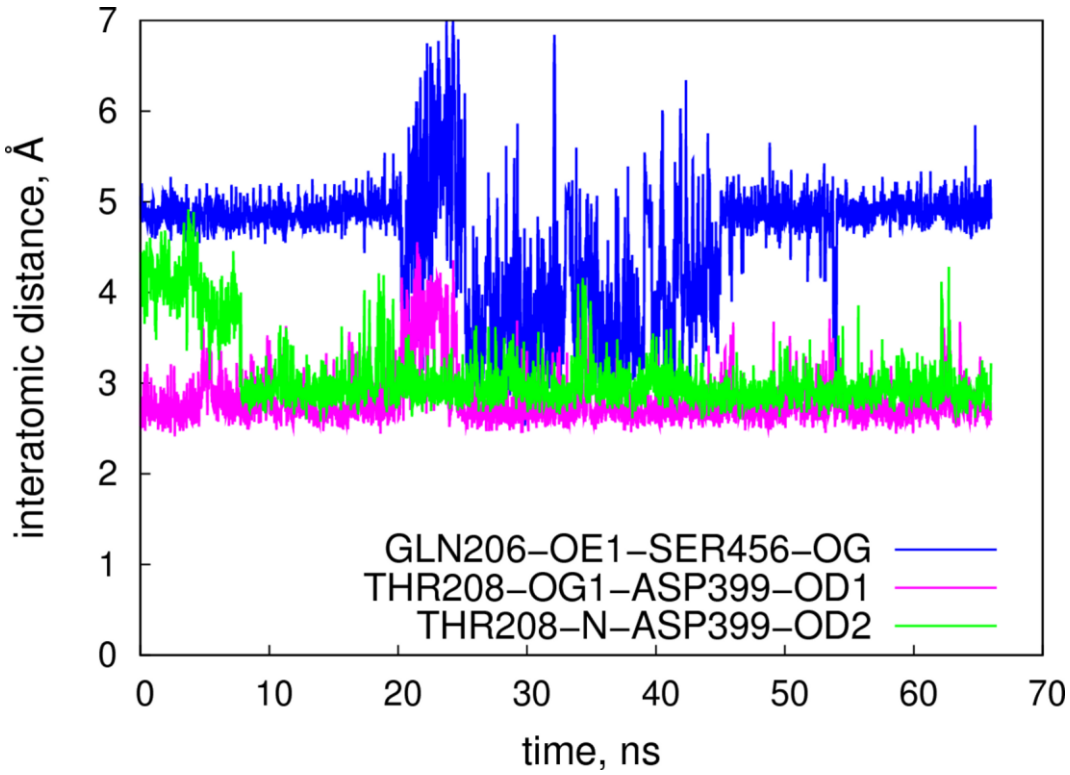

Fig. 4b

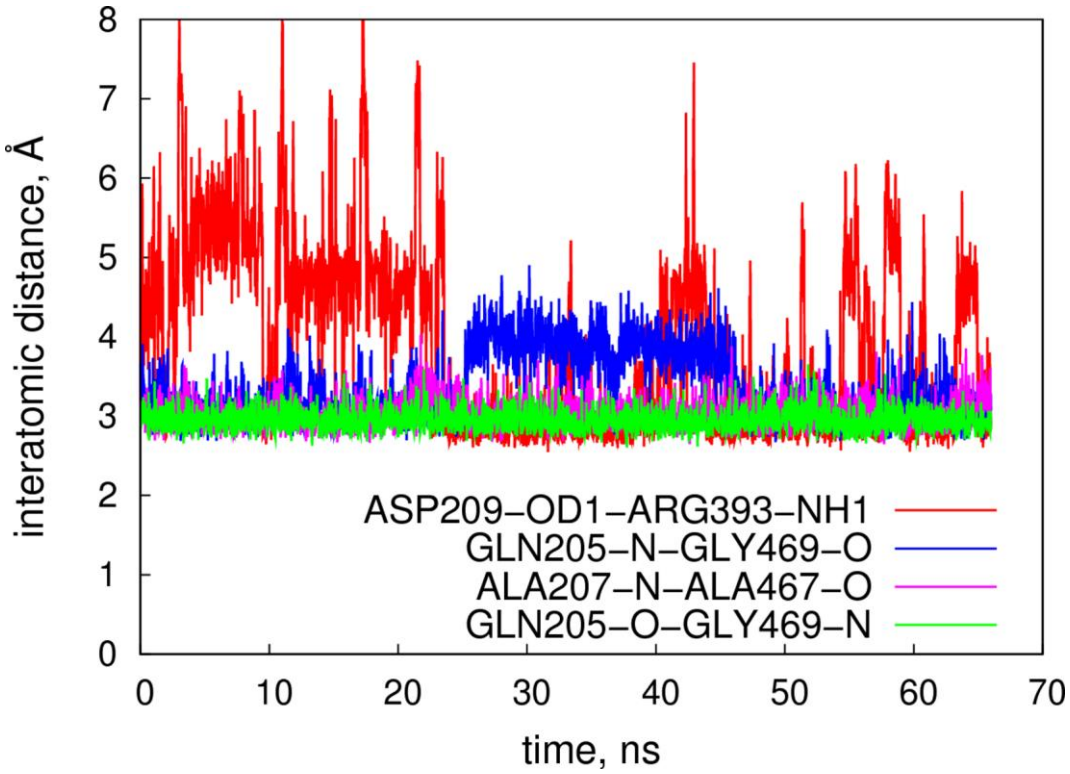

Fig. 4c

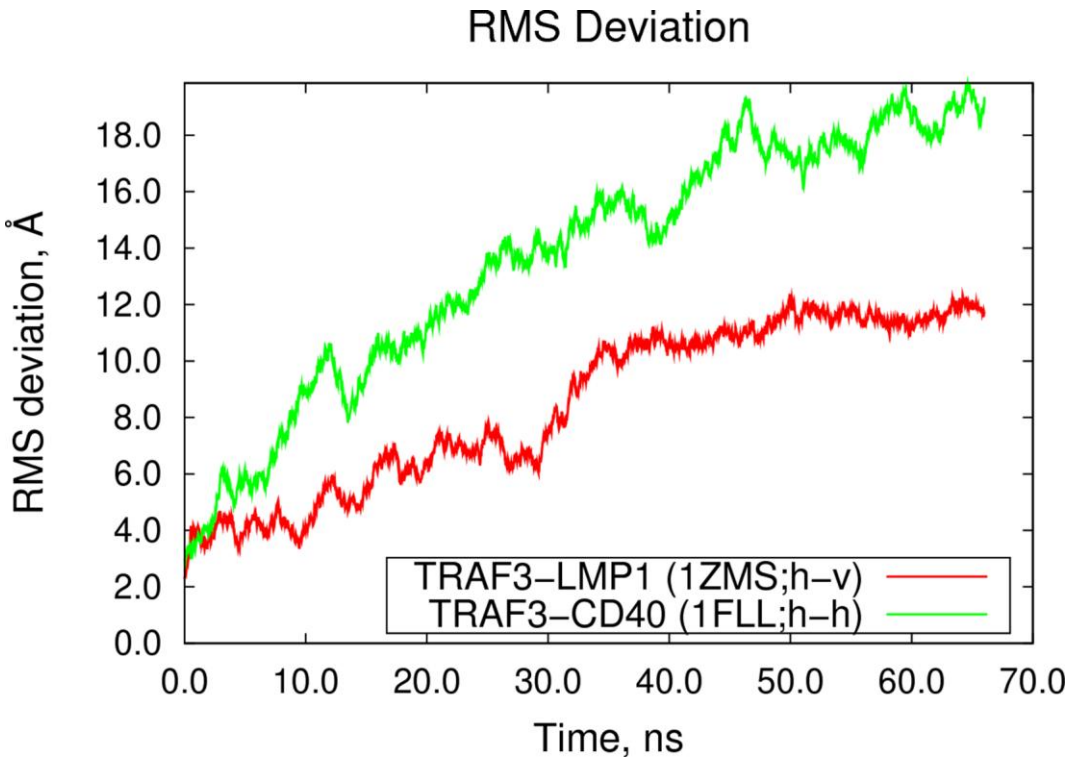

Fig. 5a

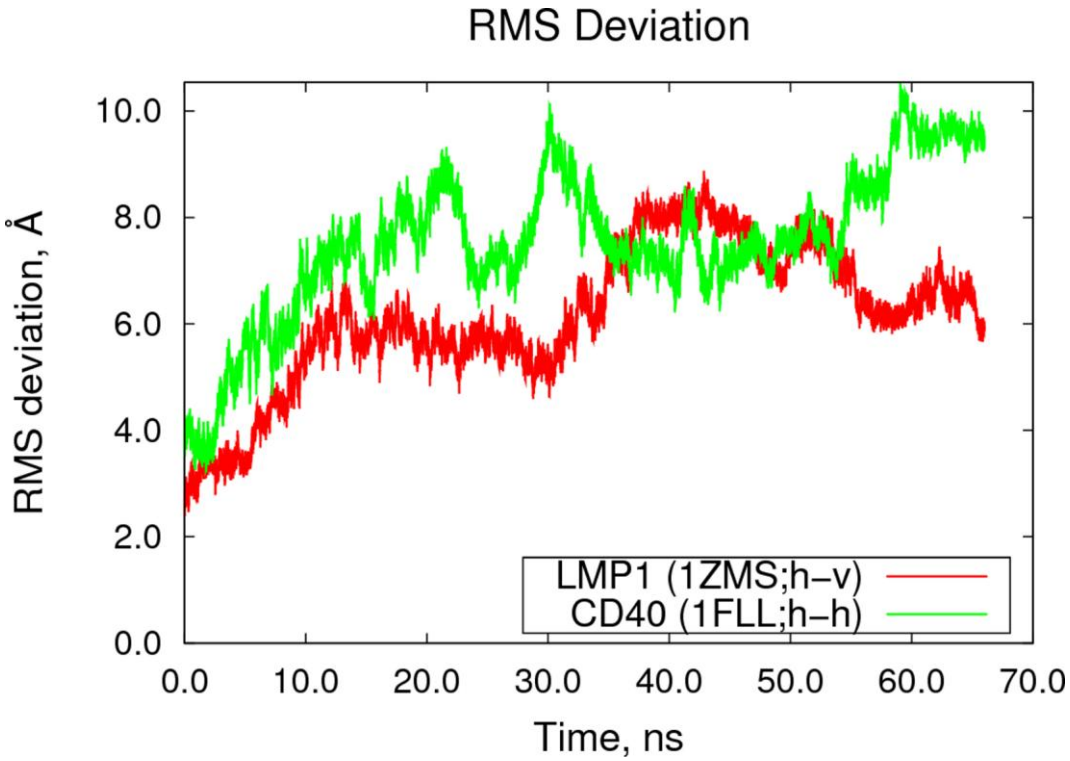

Fig. 5b

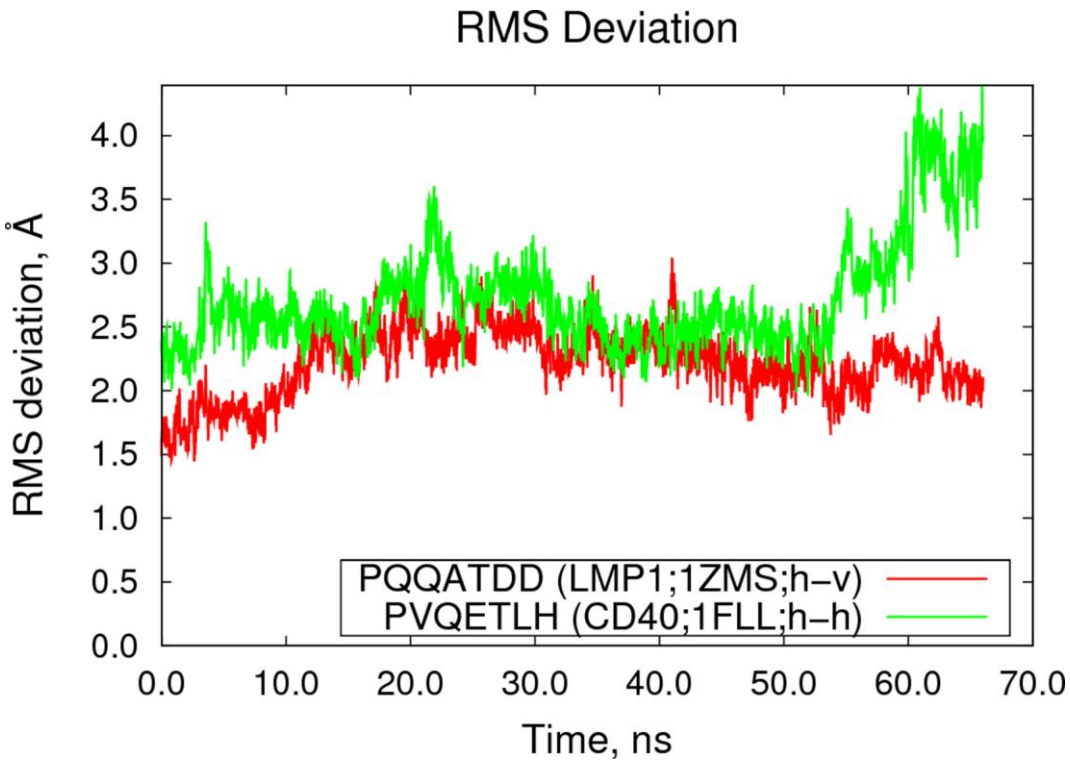

Fig. 5c

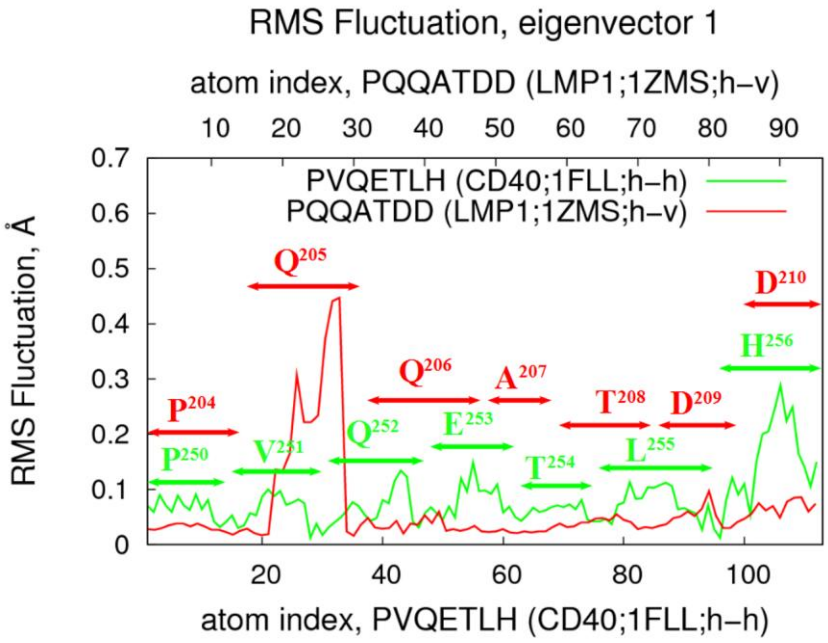

Fig. 6

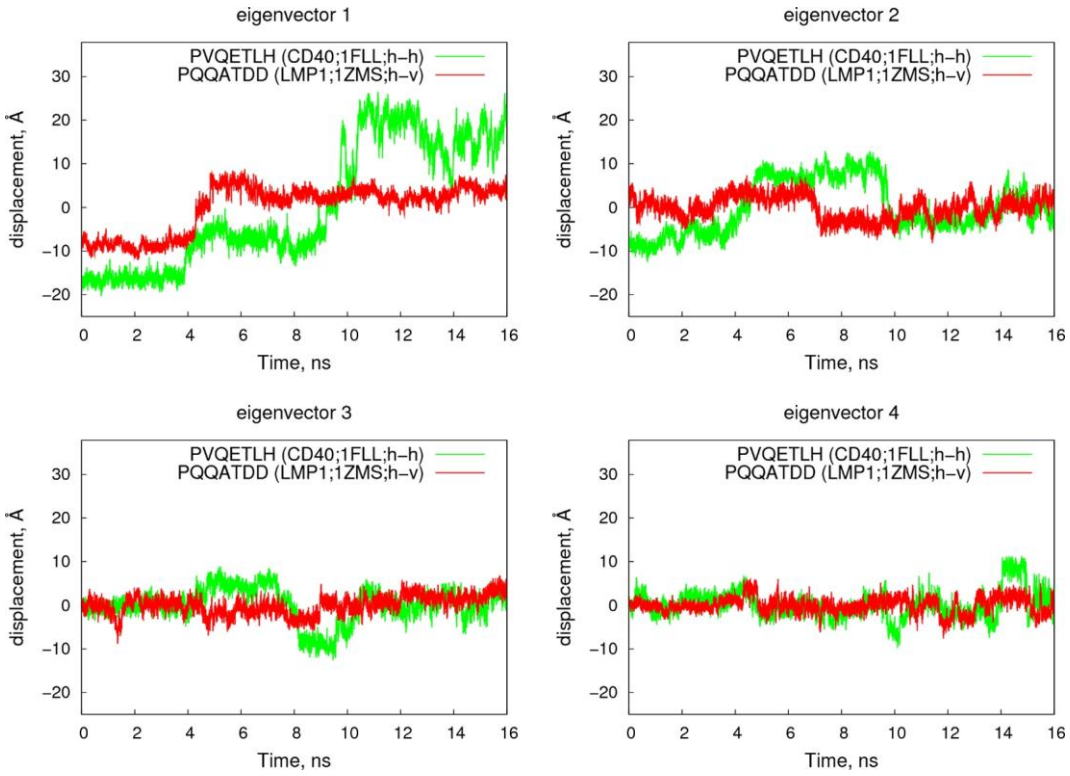

Fig. 7

Figure Captions

Fig. 1 (a) A 66.0-ns average structure of the CD40-TRAF3 complex. The Val 251-Gly 469 and Glu 253-Ala 467 hydrogen bonds are novel interactions not found in the X-ray crystallographic study (compare with Fig. 1b). (b) Intra- and intermolecular hydrogen bond interactions made by CD40 with TRAF3. The structure is derived directly from chains A and X of the PDB structure 1FLL without further alteration. Hydrogen bonds are identified automatically using the UCSF Chimera [26] software and depicted as red dashed lines. The TRAF3 secondary structure is depicted in purple while that of CD40 is depicted in green. CD40 residues are shown as tubes when necessary. Residues shown as sticks are TRAF3 residues

Fig. 2 Temporal profile of some important intra- and intermolecular hydrogen bonds made by CD40 with TRAF3. The atom labels are those for Amber. See Table 2 for details.

Fig. 3 (a) A 66.0-ns average structure of the LMP1-TRAF3 complex. The Arg 393-Asp 209 hydrogen bond is a novel interaction not found in the X-ray crystallographic study (compare with Fig. 3b). (b) Intra- and intermolecular hydrogen bond interactions made by LMP1 with TRAF3. The structure is derived directly from the PDB structure 1ZMS without further alteration. Hydrogen bonds are identified automatically using the UCSF Chimera [26] software and depicted as red dashed lines. The TRAF3 secondary structure is depicted in sky blue while that of LMP1 is depicted in red. LMP1 residues are shown as tubes when necessary. Residues shown as sticks are TRAF3 residues

Fig. 4 Temporal profile of some important intra- and intermolecular hydrogen bonds made by LMP1 with TRAF3. The atom labels are those for Amber. See Table 2 for details.

Fig. 5 RMS deviation of (a) TRAF3 complexes with CD40 and LMP1 (b) LMP1 and CD40 chains only (c) PXQXTXX consensus sequence with respect to the optimized geometry. The movement of atoms not part of the subset are ignored in the calculation of the RMSD

Fig. 6 RMS fluctuation of the first eigenvector with the largest eigenvalue, the most relevant function-related mode as revealed by essential dynamics (ED) analysis

Fig. 7 Motions along the first four eigenvectors obtained from the covariance matrix of the PXQXTXX sequence coordinates

References

1. Bailey RE (1994) Diagnosis and treatment of infectious-mononucleosis. Am Fam Physician 49 (4):879-885

2. Iwatsuki K, Satoh M, Yamamoto T, Oono T, Morizane S, Ohtsuka M, Xu ZG, Suzuki D, Tsuji K (2006) Pathogenic link between hydroa vacciniforme and Epstein-Barr virus-associated hematologic disorders. Arch Dermatol 142 (5):587-595

3. Goldgeier MH, Nordlund JJ, Lucky AW, Sibrack LA, McCarthy MJ, McGuire J (1982) Hydroa vacciniforme - diagnosis and therapy. Arch Dermatol 118 (8):588-591

4. Gupta G, Man I, Kemmett D (2000) Hydroa vacciniforme: A clinical and follow-up study of 17 cases. J Am Acad Dermatol 42 (2):208-213

5. Shibata Y, Hoshino Y, Hara S, Yagasakip H, Kojima S, Nishiyama Y, Morishima T, Kimura H (2006) Clonality analysis by sequence variation of the latent membrane protein 1 gene in patients with chronic active Epstein-Barr virus infection. J Med Virol 78 (6):770-779. doi:10.1002/jmv.20622

6. Kaye KM, Izumi KM, Kieff E (1993) Epstein-Barr virus latent membrane protein 1 is essential for B-lymphocyte growth transformation. Proceedings of the National Academy of Sciences of the United States of America 90 (19):9150-9154

7. Eliopoulos AG, Dawson CW, Mosialos G, Floettmann JE, Rowe M, Armitage RJ, Dawson J, Zapata JM, Kerr DJ, Wakelam MJO, Reed JC, Kieff E, Young LS (1996) CD40-induced growth inhibition in epithelial cells is mimicked by Epstein-Barr virus-encoded LMP1: Involvement of TRAF3 as a common mediator. Oncogene 13 (10):2243-2254

8. Foy TM, Aruffo A, Bajorath J, Buhlmann JE, Noelle RJ (1996) Immune Regulation by CD40 and its Ligand GP39. Annual Review of Immunology 14 (1):591-617. doi:doi:10.1146/annurev.immunol.14.1.591

9. Banchereau J, Bazan F, Blanchard D, Briere F, Galizzi JP, van Kooten C, Liu YJ, Rousset F, Saeland S (1994) The CD40 Antigen and its Ligand. Annual Review of Immunology 12 (1):881-926. doi:doi:10.1146/annurev.iy.12.040194.004313

10. Clark EA, Ledbetter JA (1994) How B and T cells talk to each other. Nature 367 (6462):425-428

11. Natoli G, Costanzo A, Ianni A, Templeton DJ, Woodgett JR, Balsano C, Levrero M (1997) Activation of SAPK/JNK by TNF Receptor 1 Through a Noncytotoxic TRAF2-Dependent Pathway. Science 275 (5297):200-203. doi:10.1126/science.275.5297.200

12. Liu Z-g, Hsu H, Goeddel DV, Karin M (1996) Dissection of TNF Receptor 1 Effector Functions: JNK Activation Is Not Linked to Apoptosis While NF-[kappa]B Activation Prevents Cell Death. Cell 87 (3):565-576

13. Grammer AC, Swantek JL, McFarland RD, Miura Y, Geppert T, Lipsky PE (1998) TNF Receptor-Associated Factor-3 Signaling Mediates Activation of p38 and Jun N-Terminal Kinase, Cytokine Secretion, and Ig Production Following Ligation of CD40 on Human B Cells. The Journal of Immunology 161 (3):1183-1193

14. Leo E, Welsh K, Matsuzawa S-i, Zapata JM, Kitada S, Mitchell RS, Ely KR, Reed JC (1999) Differential Requirements for Tumor Necrosis Factor Receptor-associated Factor Family Proteins in CD40-mediated Induction of NF-kappa B and Jun N-terminal Kinase Activation. Journal of Biological Chemistry 274 (32):22414-22422. doi:10.1074/jbc.274.32.22414

15. Izumi K, Kaye K, Kieff E (1997) The Epstein-Barr virus LMP1 amino acid sequence that engages tumor necrosis factor receptor associated factors is critical for primary B lymphocyte growth transformation. Proceedings of the National Academy of Sciences of the United States of America 94 (4):1447-1452

16. Wu S, Xie P, Welsh K, Li C, Ni C-Z, Zhu X, Reed JC, Satterthwait AC, Bishop GA, Ely KR (2005) LMP1 Protein from the Epstein-Barr Virus Is a Structural CD40 Decoy in B Lymphocytes for Binding to TRAF3. J Biol Chem 280 (39):33620-33626. doi:10.1074/jbc.M502511200

17. Ni C-Z, Welsh K, Leo E, Chiou C-k, Wu H, Reed JC, Ely KR (2000) Molecular basis for CD40 signaling mediated by TRAF3. Proceedings of the National Academy of Sciences of the United States of America 97 (19):10395-10399

18. Li C, Norris PS, Ni C-Z, Havert ML, Chiong EM, Tran BR, Cabezas E, Reed JC, Satterthwait AC, Ware CF, Ely KR (2003) Structurally Distinct Recognition Motifs in Lymphotoxin-{beta} Receptor and CD40 for Tumor Necrosis Factor Receptor-associated Factor (TRAF)-mediated Signaling. J Biol Chem 278 (50):50523-50529. doi:10.1074/jbc.M309381200

19. Ni CZ, Oganesyan G, Welsh K, Zhu XW, Reed JC, Satterthwait AC, Cheng GH, Ely KR (2004) Key molecular contacts promote recognition of the BAFF receptor by TNF receptor-associated factor 3: Implications for intracellular signaling regulation. J Immunol 173 (12):7394-7400

20. Amadei A, Linssen ABM, Berendsen HJC (1993) Essential dynamics of proteins. Proteins: Structure, Function, and Genetics 17 (4):412-425

21. Pearlman DA, Case DA, Caldwell JW, Ross WS, Cheatham TE, DeBolt S, Ferguson D, Seibel G, Kollman P (1995) AMBER, a package of computer programs for applying molecular mechanics, normal mode analysis, molecular dynamics and free energy calculations to simulate the structural and energetic properties of molecules. Computer Physics Communications 91 (1-3):1-41

22. Case DA, Cheatham TE, Darden T, Gohlke H, Luo R, Merz KM, Onufriev A, Simmerling C, Wang B, Woods RJ (2005) The Amber biomolecular simulation programs. Journal of Computational Chemistry 26 (16):1668-1688. doi:10.1002/jcc.20290

23. Kirschner KN, Woods RJ (2001) Quantum Mechanical Study of the Nonbonded Forces in Water-ethanol Complexes. The Journal of Physical Chemistry A 105 (16):4150-4155. doi:10.1021/jp004413y

24. Wang J, Cieplak P, Kollman PA (2000) How well does a restrained electrostatic potential (RESP) model perform in calculating conformational energies of organic and biological molecules? Journal of Computational Chemistry 21 (12):1049-1074. doi:10.1002/1096-987x(200009)21:12<1049::aid-jcc3>3.0.co;2-f

25. Cornell WD, Cieplak P, Bayly CI, Gould IR, Merz KM, Ferguson DM, Spellmeyer DC, Fox T, Caldwell JW, Kollman PA (1995) A Second Generation Force Field for the Simulation of Proteins, Nucleic Acids, and Organic Molecules. Journal of the American Chemical Society 117 (19):5179-5197. doi:10.1021/ja00124a002

26. Pettersen EF, Goddard TD, Huang CC, Couch GS, Greenblatt DM, Meng EC, Ferrin TE (2004) UCSF Chimera—A visualization system for exploratory research and analysis. Journal of Computational Chemistry 25 (13):1605-1612. doi:10.1002/jcc.20084

27. Mills JEJ, Dean PM (1996) Three-dimensional hydrogen-bond geometry and probability information from a crystal survey. Journal of Computer-Aided Molecular Design 10 (6):607-622. doi:10.1007/bf00134183

Supplementary Information

An MD simulation of the decoy action of Epstein-Barr virus LMP1 protein mimicking the CD40 interaction with TRAF3

Wilfredo Credo Chung • Toshimasa Ishida

Fukui Institute for Fundamental Chemistry, Kyoto University,
34-4, Takano-nishihirakicho, Sakyo-ku, Kyoto 606-8103, Japan

S1 Introduction

To confirm that the observations made here based on a single 66-ns trajectory is statistically representative enough and not a consequence of chance, we also calculated six 2-ns trajectories and analyzed them as usual. Whereas it is desirable to calculate several tens-of-nanoseconds trajectories in order to get a clearer picture of the dynamics, such an undertaking would need computational resources not available to us at present. It will be shown here that indeed the early-stage dynamics of the 66-ns trajectory is reflected in the short-time trajectories.

S2 Results and Discussion

S2.1 CD40-TRAF3 interactions

Six 2-ns trajectories were calculated under the same simulation conditions but using a different random number seed for the random number generator to which the initial MD velocity assigned during the heating process is dependent. The temporal profile of the interatomic distances that are monitored in the 66-ns trajectory is similar. For instance, the length of the hydrogen bonds that are revealed by the 66-ns MD trajectory (see Table 2(a) and Fig. 1(a) of the main article) remained short during the 2-ns period of the short trajectory (see red lines, Fig. S1) as it is during the first 2 ns of the 66-ns trajectory (see black line, Fig. S1). This is specially true for the novel interaction between CD40 Glu 253's backbone amido N and TRAF3 Val 251's backbone carbonyl O (Fig. S1(a)). The hydrogen bond between CD40 Val 251 and TRAF3 Gly 469 would not be formed until after ~8 ns later (see green line, Fig 2(b) of the main article) and thus its temporal profile is understandably erratic during the first 2 ns (see Fig S1(b) and (c)).

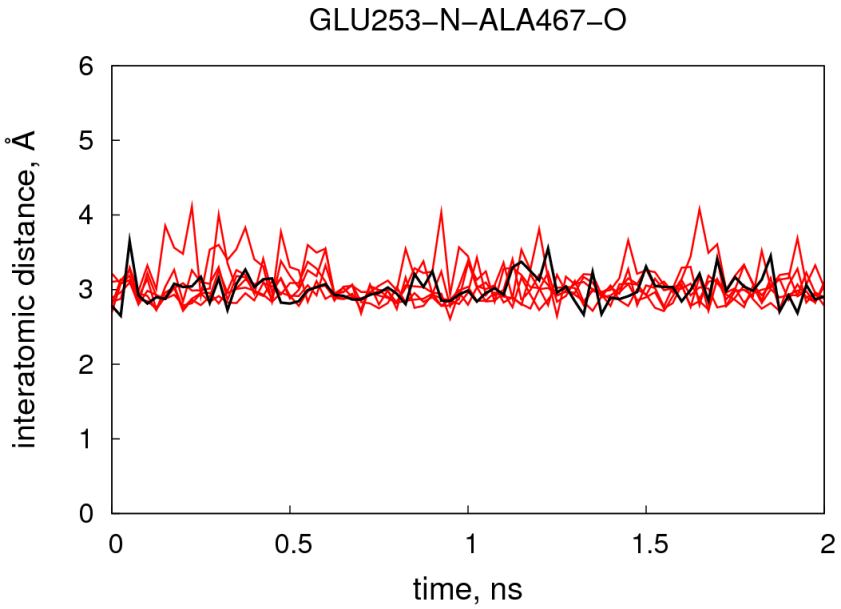

(a)

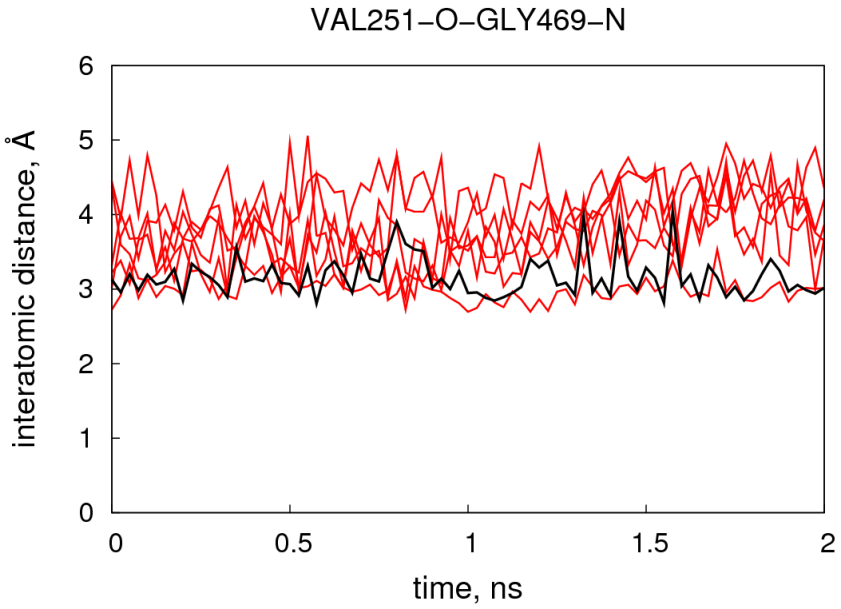

(b)

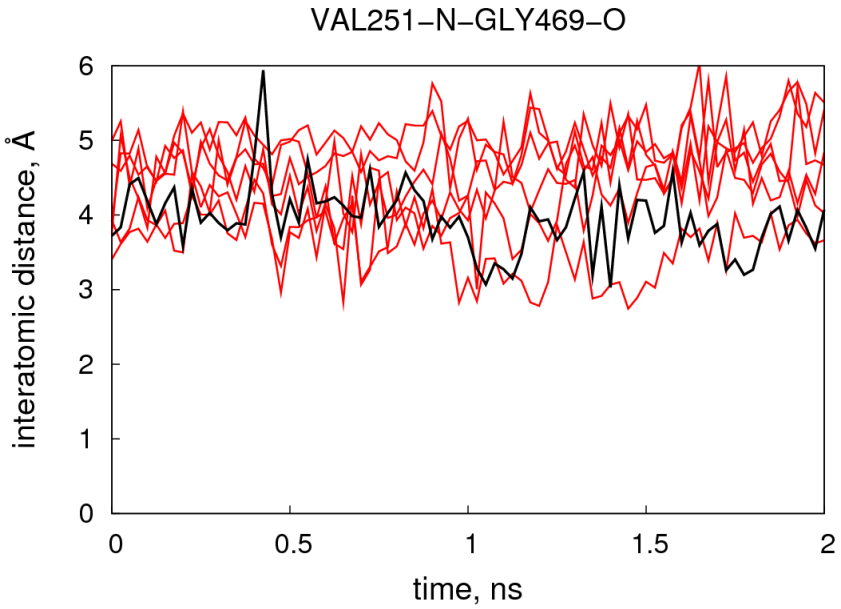

(c)

Figure S1 Temporal profile of some important intra- and intermolecular hydrogen bonds made by CD40 with TRAF3. Standard Amber atom names are used: N = backbone amido N; O = backbone carbonyl O; OG = Ser hydroxyl O; OD1/OD2 = Asp side-chain carboxyl O; OE1 = Glu/Gln carboxyl O; OH = Tyr hydroxyl O; OG1 = Thr hydroxyl O. The black line is from the 66-ns trajectory. The red lines are from the 2-ns trajectories.

The hydrogen bonds that are eventually broken in the 66-ns MD simulation (see Table 2; see also Fig. 2(a)) show early signs of being broken (see black lines, Fig. S2(a) and (b)). This behavior is also replicated by the 2-ns MD trajectories (see Fig. S2(a) and (b)). The interatomic distances in Fig. S2 are relatively shorter than what would be achieved after some tens of nanoseconds (see Fig. 2(a) of the main article). It is found, however, that the pattern shown by the 66-ns trajectory during the first 2 ns (black line, Fig. S2(a) and (b)) is more or less average of the ensemble of trajectories and thus it is anticipated that the other trajectories would also exhibit a similar dynamics at longer periods if allowed to proceed.

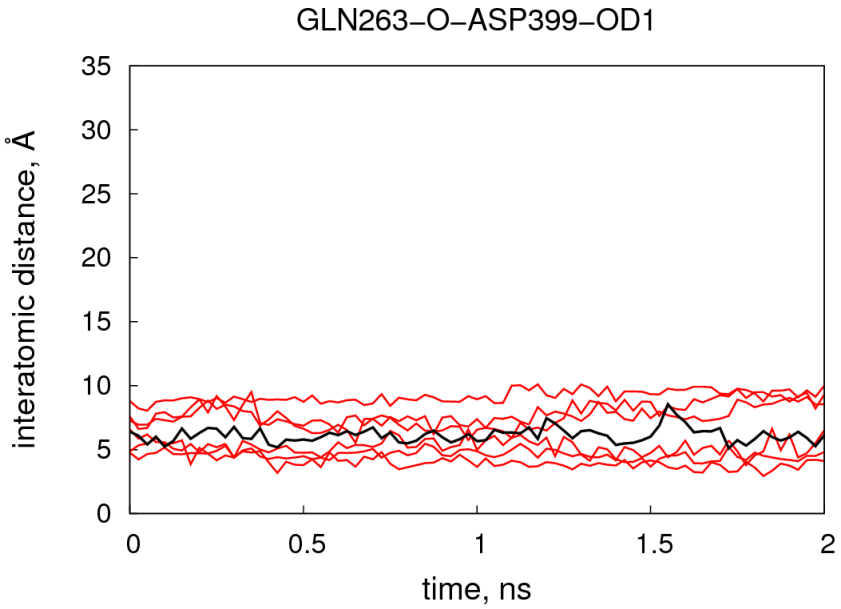

(a)

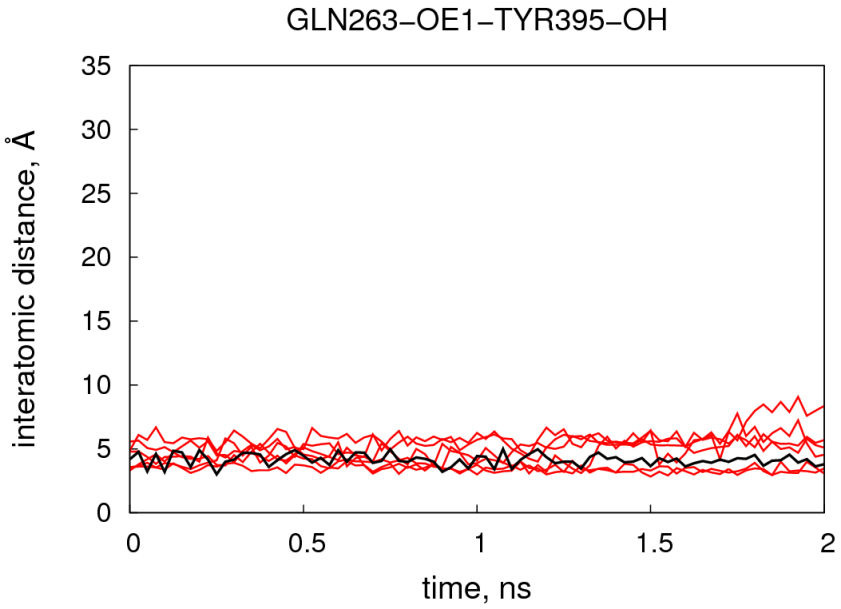

(b)

Figure S2 Temporal profile of some important intra- and intermolecular hydrogen bonds made by CD40 with TRAF3. Standard Amber atom names are used. See Figure S1 for details. The black line is from the 66-ns trajectory. The red lines are from the 2-ns trajectories.

The average structure of the 2-ns trajectory (Fig. S3) invariably supports our claim that the single 66-ns trajectory is sufficiently representative of the ensemble. The crucial hydrogen bonds are essentially formed already within the 2-ns period (see red dashed line, Fig. S3; compare with Fig. 1(a) of the main article). Also, the hydrogen bonds originally made by TRAF3's Tyr 395 and Asp 399 are already severed at this time. Although the hairpin loop still looks intact, the hydrogen bond that holds the structure (between Thr 254 and Gln 264 is already broken. It is anticipated that the hairpin loop will eventually be destroyed as it is in the 66-ns trajectory.

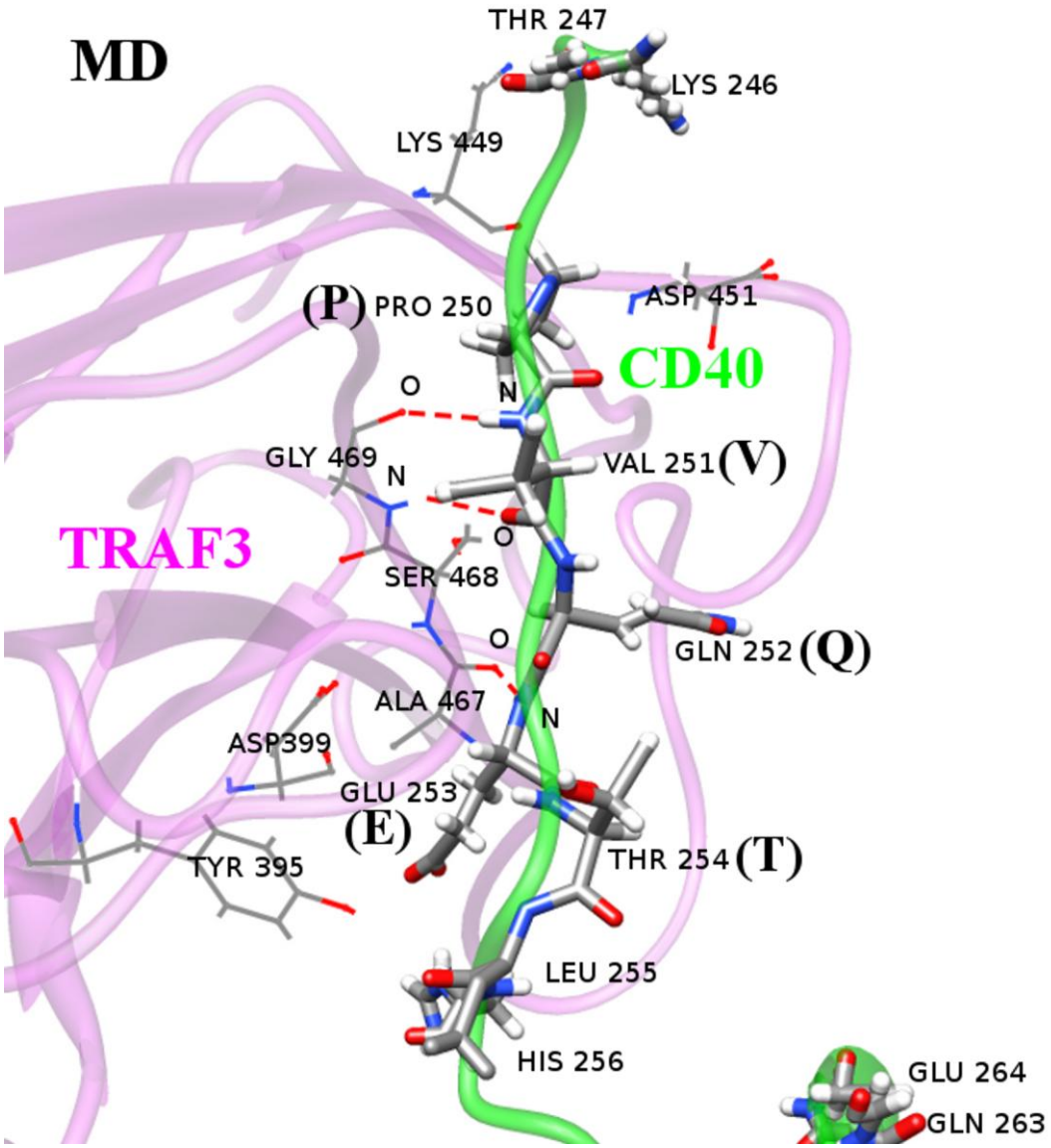

(a) average of 66-ns trajectory

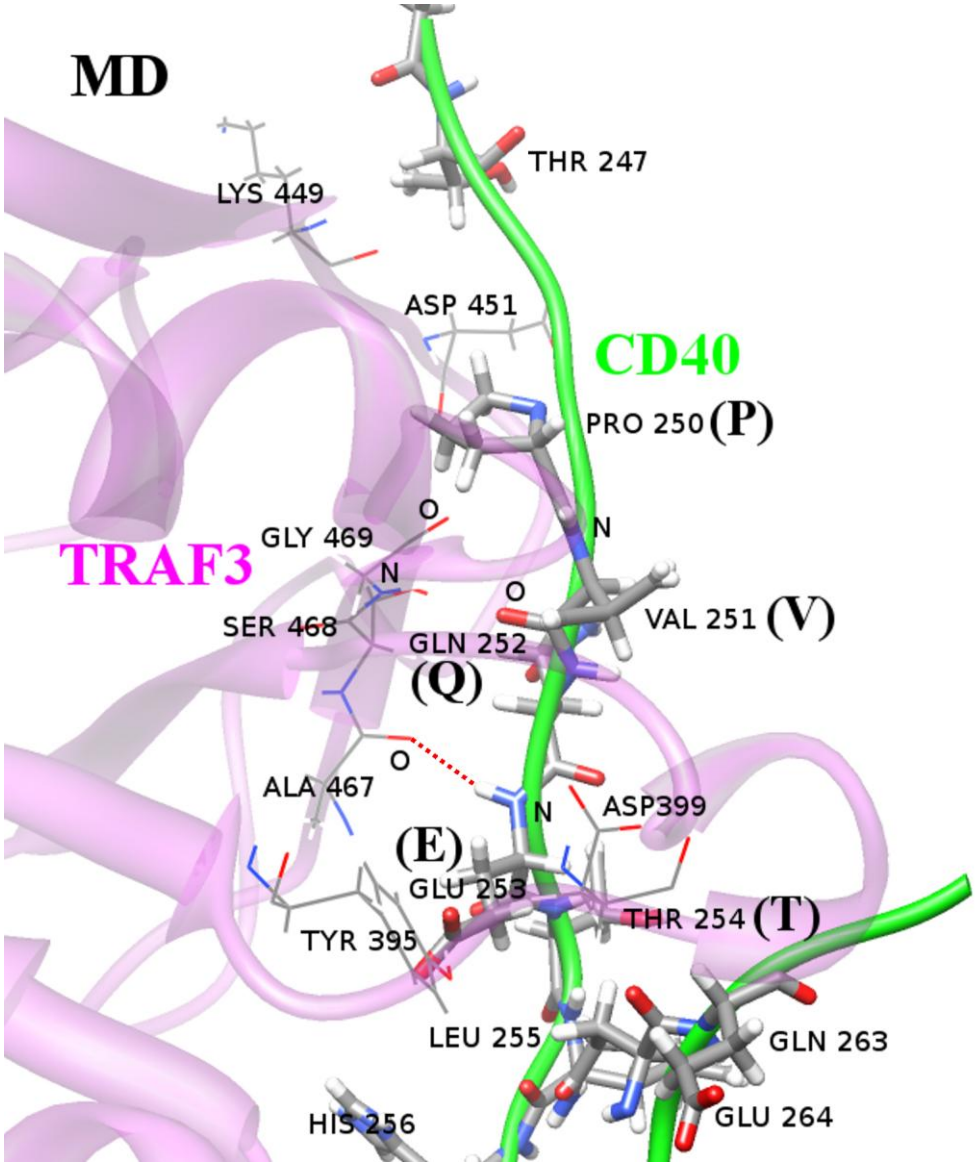

(b) average of six 2-ns trajectories

Figure S3 Average structure of the CD40-TRAF3 complex. Hydrogen bonds are identified automatically using the UCSF Chimera software and depicted as red dashed lines. The TRAF3 secondary structure is depicted in purple while that of CD40 is depicted in green. CD40 residues are shown as tubes when necessary. Residues shown as sticks are TRAF3 residues

S2.2 LMP1-TRAF3 interactions

As we did in the simulation of the TRAF3-CD40 interaction, six short trajectories are also calculated for the TRAF3-LMP1 case. As is the case in the TRAF3-CD40 interactions, the dynamics of the 2-ns trajectory closely resembles that of the initial 2 ns of the 66-ns simulation. The five hydrogen bonds between TRAF3 and LMP1 that are originally identified in the X-ray structure and remained strong after solvation and thermal equilibration (see Table 2(b); see also Fig. 4(b), 4(c) of the main article and Fig. S4(a)-(c)) demonstrate strength during the 2-ns period of the short simulation (see Fig. S4 and S5) The hydrogen bond between Asp 209 and Arg 393 is

rather erratic and this behavior is also reflected in the short trajectories (Fig. S5(a)). The hydrogen bond between Thr 208 N and Asp 399 OD2 is not re-established until after ~10 ns in the 66-ns trajectory (see green line, Fig 4(b) of the main article). In the 2-ns trajectories, on the other hand, it remains relatively intact (see red lines, Fig S5(b)). The three hydrogen bonds that are revealed in the X-ray structure but are destroyed in the thermally-equilibrated structure (see Table 2(b); see also Figure 4(a) of the main article) are broken early in the both in the 66-ns trajectory and the 2-ns simulations (see Fig. S6).

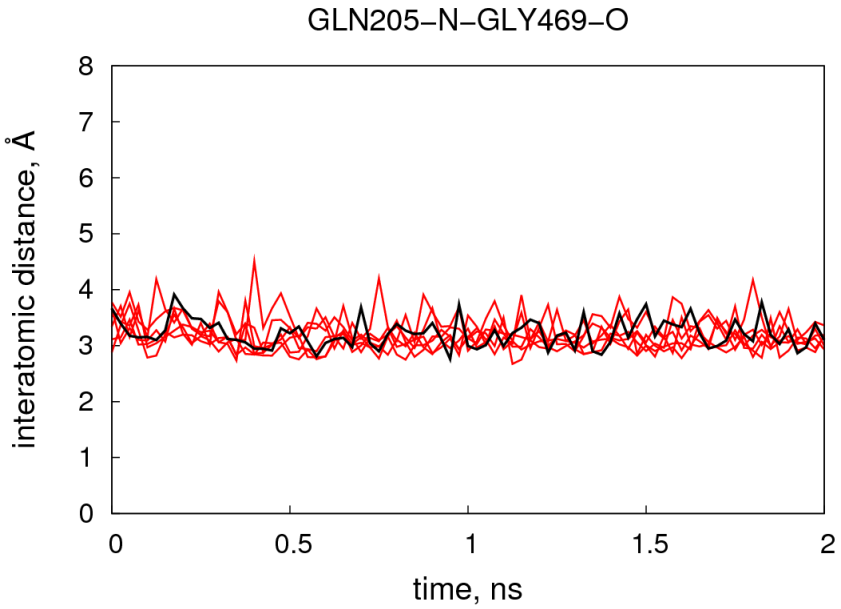

(a)

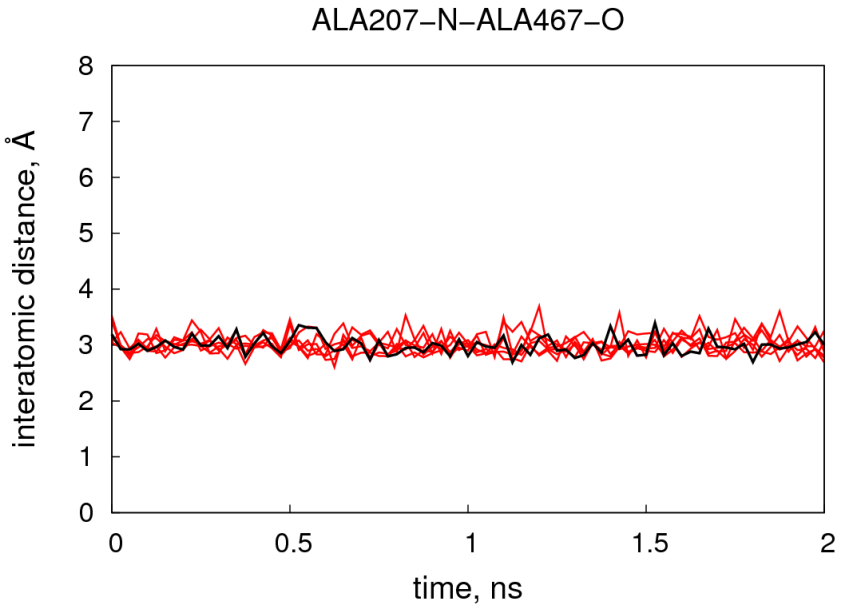

(b)

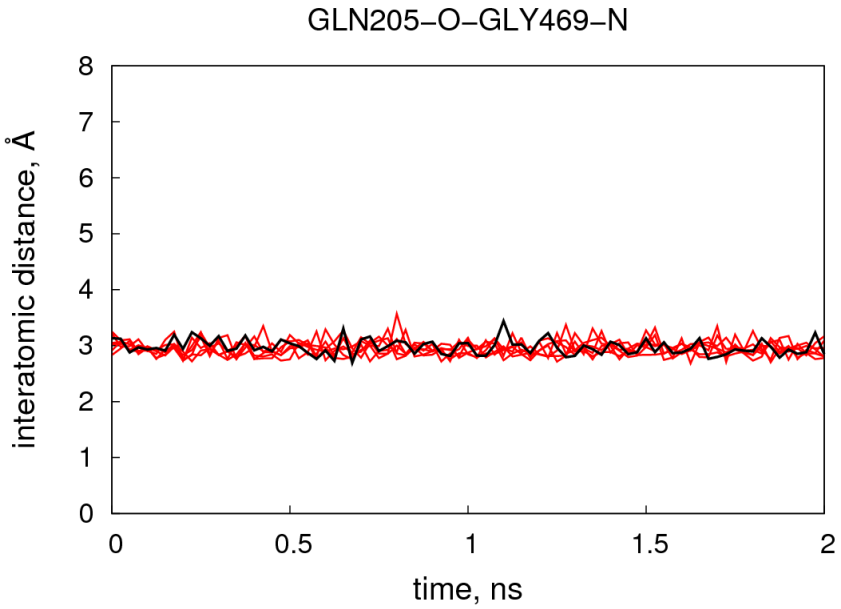

(c)

Figure S4 Temporal profile of some important intra- and intermolecular hydrogen bonds made by LMP1 with TRAF3. Standard Amber atom names are used. See Figure S1 for details. The black line is from the 66-ns trajectory. The red lines are from the 2-ns trajectories.

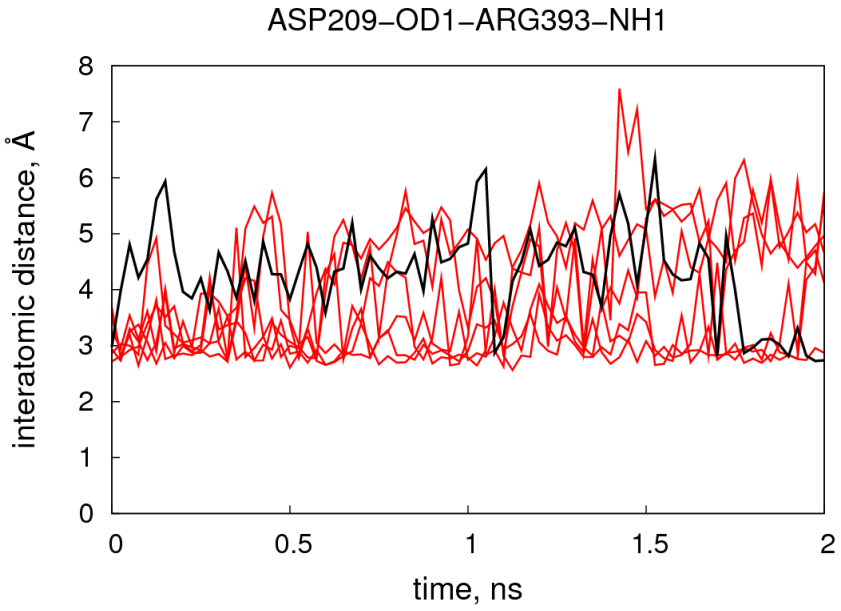

(a)

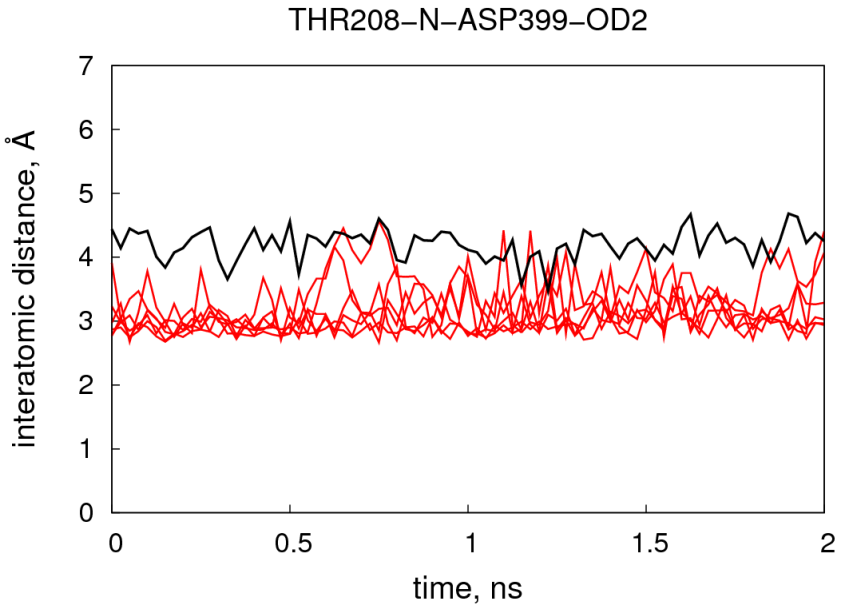

(b)

Figure S5 Temporal profile of some important intra- and intermolecular hydrogen bonds made by LMP1 with TRAF3. Standard Amber atom names are used. See Figure S1 for details. The black line is from the 66-ns trajectory. The red lines are from the 2-ns trajectories.

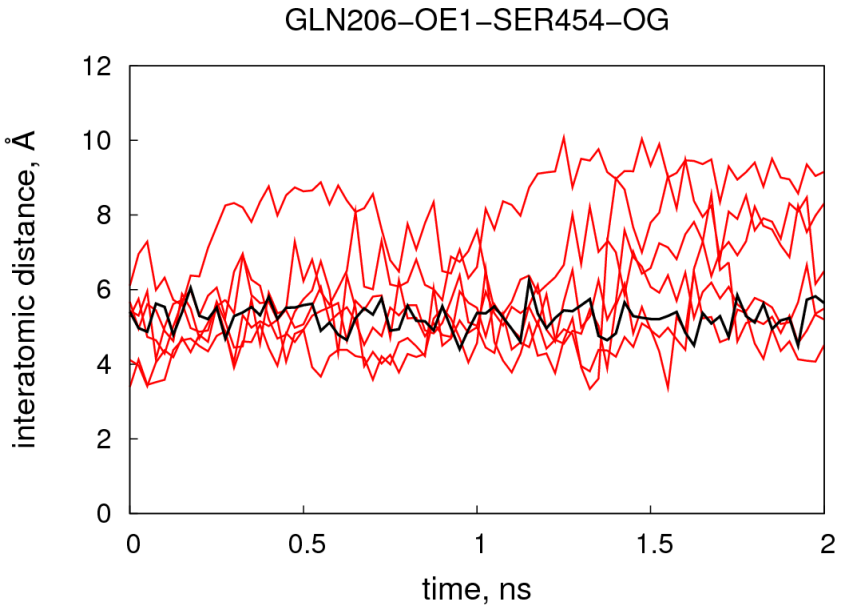

(a)

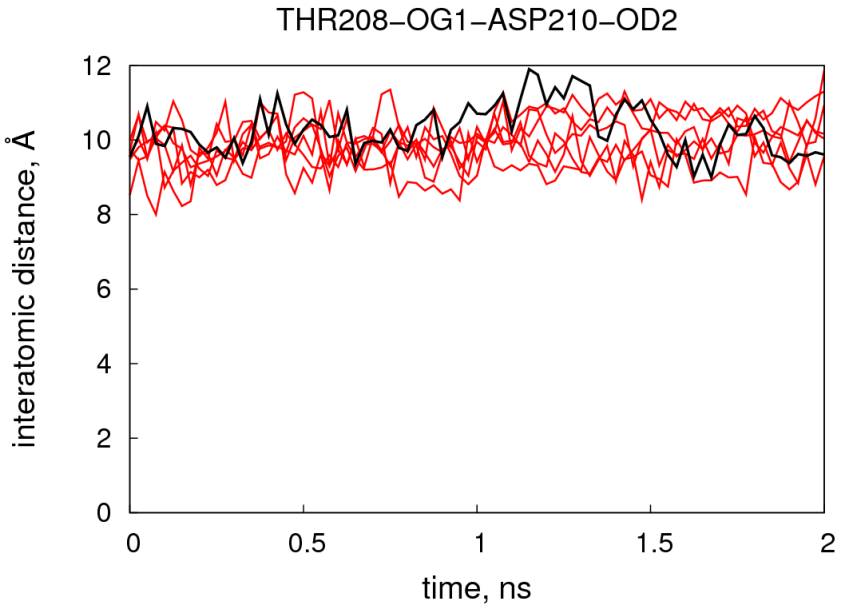

(b)

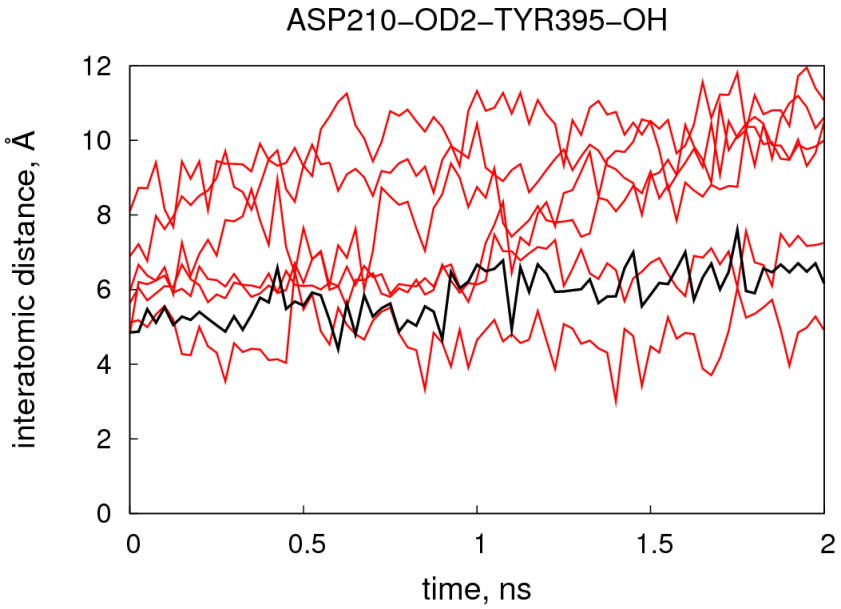

(c)

Figure S6 Temporal profile of some important intra- and intermolecular hydrogen bonds made by LMP1 with TRAF3. Standard Amber atom names are used. See Figure S1 for details. The black line is from the 66-ns trajectory. The red lines are from the 2-ns trajectories.

The average structure of the 2-ns TRAF3-LMP1 trajectories (Fig. S7(b)) is likewise supportive of the observation that the single 66-ns trajectory is representative of an ensemble of trajectories. Comparing Figures 7(a) and 7(b) reveals striking similarities. The average structure of the 2-ns trajectories reveal a partially formed bidental-type hydrogen bond network between LMP1 Gln 205 and TRAF3 Gly 469. Also, the new hydrogen bond between LMP1 Ala 207 and TRAF3 Ala 467 is already stable at this time. The hydrogen bond between LMP1 Gln 206 and TRAF3 Ser 456 is already severed during the 2-ns period, at is is in the first 2 ns of the 66-ns simulation.

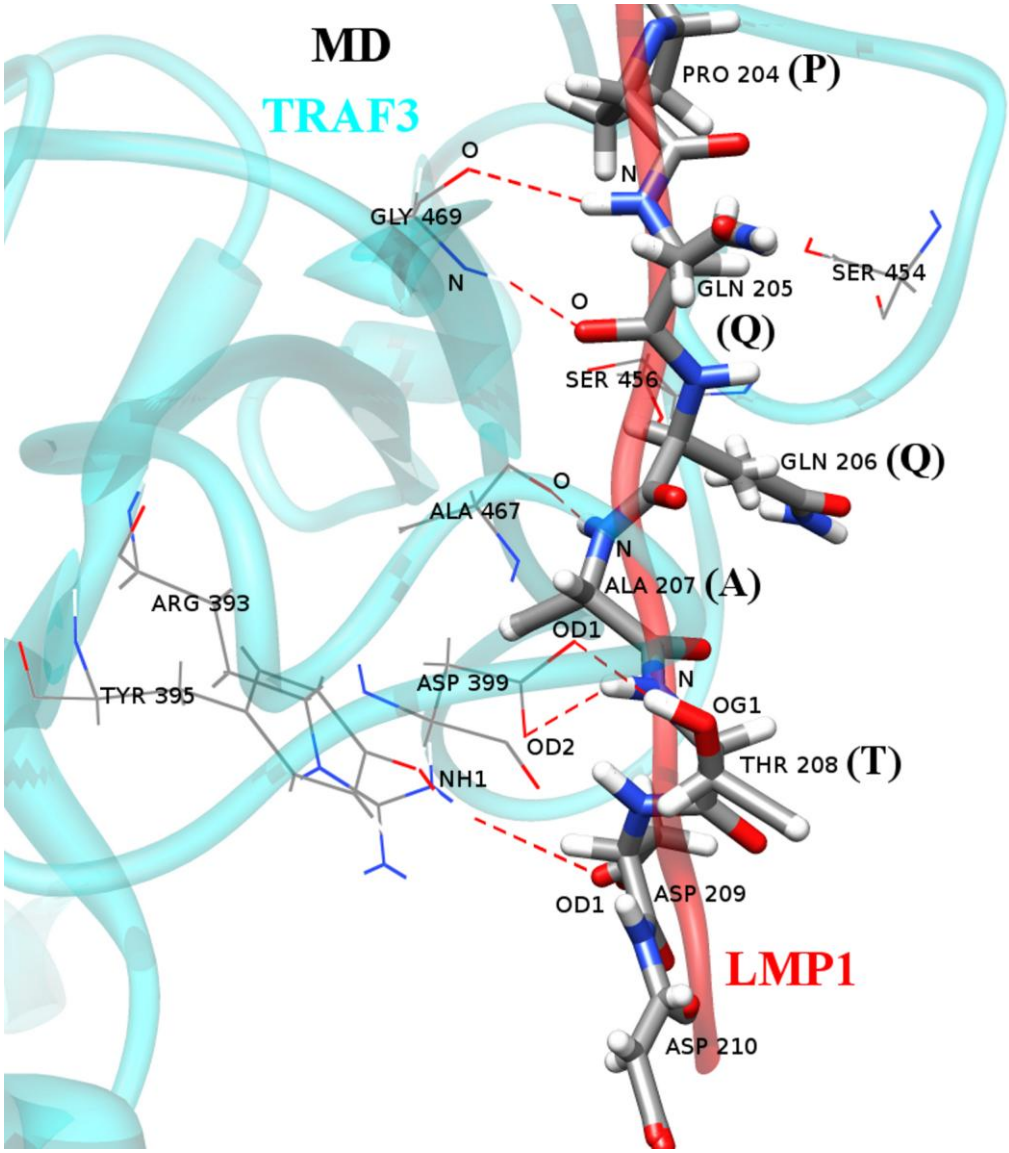

(a) average of 66-ns trajectory

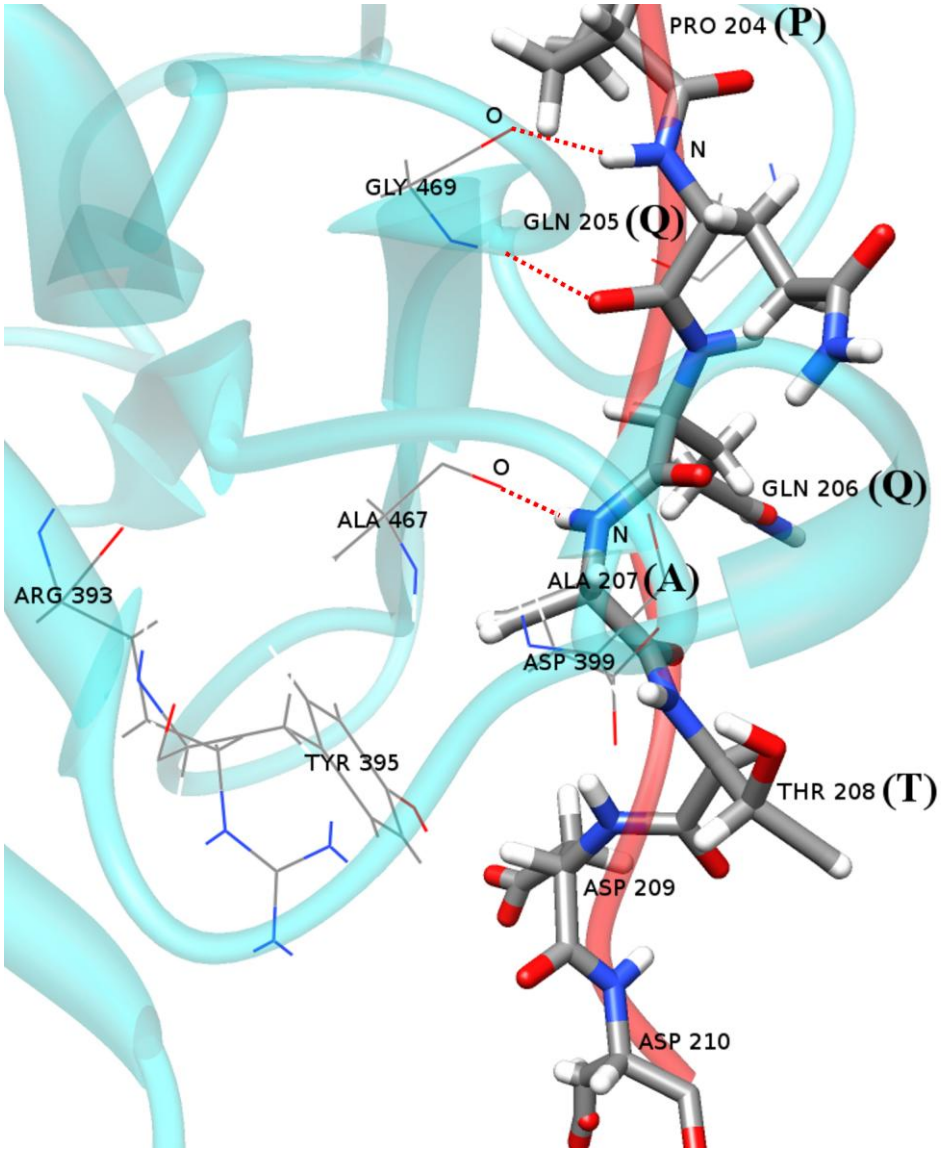

(b) average of six 2-ns trajectories

Figure S7 Average structure of the LMP1-TRAF3 complex. Hydrogen bonds are identified automatically using the UCSF Chimera software and depicted as red dashed lines. The TRAF3 secondary structure is depicted in sky blue while that of LMP1 is depicted in red. LMP1 residues are shown as tubes when necessary. Residues shown as sticks are TRAF3 residues

S3 Conclusion

Thus while in the main article we discussed in detail the results of a single 66-ns trajectory, the observations cannot be accidental in nature since the results taken from an ensemble of short-time trajectories coincide with the early-stage dynamics of the long-time trajectory.